ever, the Japanese patients received both surgery and a large array of antimycobacterial drugs (Table 7). In addition, in Africa, most patients who had lesions with cross-sectional diameters of ≤10 cm showed excellent healing without surgery (17). Although the *in vitro* susceptibilities of the Japanese isolates to streptomycin, kanamycin, and clarithromycin are higher than those of the *M. ulcerans* strains from West Africa (Table 6), treatment has been fairly aggressive in Japan. It is speculated that because the majority of doctors and patients in Japan have not experienced and cannot recognize Buruli ulcer disease, they might fear the progression and recurrence of disease. Especially when patients complain of pain (9 patients in this study [47%] experienced pain [Fig. 4]), their doctors and family members are willing to initiate aggressive treatment, even in the absence of an immunodeficiency risk factor. Public information campaigns about the disease are needed, as is the establishment of guidelines for the treatment of Buruli ulcer in Japan. Clarification of the mode of transmission is also important. However, the occurrence of cases has been very sporadic, and none could be linked to an aquatic environment. Thus, the source and route of the infection remain unclear.

ACKNOWLEDGMENTS

This work was supported in part by a Grant-in-Aid for Research on Emerging and Re-emerging Infectious Diseases from the Ministry of Health, Labor, and Welfare of Japan (to Y.H., M.M., and N.I.), by a Grant-in-Aid for Scientific Research (C) from the Ministry of Education, Culture, Sports, Science and Technology of Japan (to Y.H.), and by a Grant-in-Aid for Scientific Research (C) from the Japan Society for the Promotion of Science (to K.N.).

REFERENCES

1. **Ablordey, A., et al.** 2005. Comparative nucleotide sequence analysis of polymorphic variable number tandem repeat loci in *Mycobacterium ulcerans*. J. Clin. Microbiol. **43**:5281–5284.
2. **Alsop, D. G.** 1972. The Bairnsdale ulcer. Aust. N. Z. J. Surg. **41**:317–319.
3. **Clancey, J. K., O. G. Dodge, H. F. Lunn, and M. L. Oduori.** 1961. Mycobacterial skin ulcers in Uganda. Lancet **ii**:951–954.
4. **Faber, W. R., et al.** 2000. First reported case of *Mycobacterium ulcerans* infection in a patient from China. Trans. R. Soc. Trop. Med. Hyg. **94**:277–279.
5. **Fenner, F.** 1951. The significance of the incubation period in infectious diseases. Med. J. Aust. **2**:813–818.
6. **Funakoshi, T., et al.** 2009. Intractable ulcer caused by *Mycobacterium shinshuense*: successful identification of mycobacterium strain by 16S ribosomal RNA 3′-end sequencing. Clin. Exp. Dermatol. **34**:e712–e715.
7. **Imada, H., et al.** 2008. Cutaneous ulcer of a right olecranon due to *Mycobacterium shinshuense*; a case report. Seikeigeka **59**:1440–1445. (In Japanese.)
8. **Kaminuma, E., et al.** 2010. DDBJ launches a new archive database with analytical tools for next-generation sequence data. Nucleic Acids Res. **38**(Database issue):D33–D38.
9. **Käser, M., et al.** 2007. Evolution of two distinct phylogenetic lineages of the emerging human pathogen *Mycobacterium ulcerans*. BMC Evol. Biol. **7**:177.
10. **Kazumi, Y., et al.** 2004. *Mycobacterium shinshuense* isolated from cutaneous ulcer lesion of right lower extremity in a 37-year-old woman. Kekkaku **79**:437–441. (In Japanese.)
11. **Kim, B.-J., et al.** 1999. Identification of mycobacterial species by comparative sequence analysis of the RNA polymerase gene (*rpoB*). J. Clin. Microbiol. **37**:1714–1720.
12. **Kondo, M., et al.** 2009. Leg ulcer caused by *Mycobacterium ulcerans* ssp. *shinshuense* infection. Int. J. Dermatol. **48**:1330–1333.
13. **Kusunoki, S., et al.** 1991. Application of colorimetric microdilution plate hybridization for rapid genetic identification of 22 *Mycobacterium* species. J. Clin. Microbiol. **29**:1596–1603.
14. **MacCallum, P., J. C. Tolhurst, G. Buckle, and H. I. Sissons.** 1948. A new mycobacterial infection in man. I. Clinical aspects. II. Experimental investigations in laboratory animals. III. Pathology of the experimental lesions in the rat. IV. Cultivation of the new mycobacterium. J. Pathol. Bacteriol. **60**:93–122.
15. **Mikoshiba, H., et al.** 1982. A case of atypical mycobacteriosis due to *Mycobacterium ulcerans*-like organism. Nihon Hifukagakkaizassi **92**:557–565. (In Japanese.)
16. **Nakanaga, K., et al.** 2007. "*Mycobacterium ulcerans* subsp. *shinshuense*" isolated from a skin ulcer lesion: identification based on 16S rRNA gene sequencing. J. Clin. Microbiol. **45**:3840–3843.
17. **Nienhuis, W. A., et al.** 2010. Antimicrobial treatment for early, limited *Mycobacterium ulcerans* infection: a randomized controlled trial. Lancet **375**: 664–672.
18. **Phillips, R. C., et al.** 2005. Sensitivity of PCR targeting the IS*2404* insertion sequence of *Mycobacterium ulcerans* in an assay using punch biopsy specimens for diagnosis of Buruli ulcer. J. Clin. Microbiol. **43**:3650–3656.
19. **Pidot, S. J., et al.** 2008. Deciphering the genetic basis for polyketide variation among mycobacteria producing mycolactones. BMC Genomics **9**:462.
20. **Portaels, F., et al.** 1996. Variability in 3′ end of 16S rRNA sequence of *Mycobacterium ulcerans* is related to geographic origin of isolates. J. Clin. Microbiol. **34**:962–965.
21. **Portaels, F., M. T. Silva, and W. M. Meyers.** 2009. Buruli ulcer. Clin. Dermatol. **27**:291–305.
22. **Portaels, F., P. Johnson, and W. M. Meyers (ed.).** April 2001. Buruli ulcer: diagnosis of *Mycobacterium ulcerans* disease. A manual for health care providers. World Health Organization, Geneva, Switzerland. http://whqlibdoc.who.int/hq/2001/WHO_CDS_CPE_GBUI_2001.4.pdf.
23. **Roth, A., et al.** 1998. Differentiation of phylogenetically related slowly growing mycobacteria based on 16S–23S rRNA gene internal transcribed spacer sequences. J. Clin. Microbiol. **36**:139–147.
24. **Springer, B., et al.** 1996. Isolation and characterization of a unique group of slowly growing mycobacteria: description of *Mycobacterium lentiflavum* sp. nov. J. Clin. Microbiol. **34**:1100–1107.
25. **Stinear, T. P., et al.** 2004. Giant plasmid-encoded polyketide synthases produce the macrolide toxin of *Mycobacterium ulcerans*. Proc. Natl. Acad. Sci. U. S. A. **101**:1345–1349.
26. **Stinear, T. P., et al.** 2005. Common evolutionary origin for the unstable virulence plasmid pMUM found in geographically diverse strains of *Mycobacterium* ulcerans. J. Bacteriol. **187**:1668–1676.
27. **Stragier, P., A. Ablordey, L. Durnez, and F. Portaels.** 2007. VNTR analysis differentiates *Mycobacterium ulcerans* and IS*2404* positive mycobacteria. Syst. Appl. Microbiol. **30**:525–530.
28. **Suzuki, S., et al.** 2008. Skin ulcer caused by '*Mycobacterium ulcerans* subsp. *shinshuense* ' infection. Hifubyou Shinryo **30**:145–148. (In Japanese.)
29. **Tamura, K., J. Dudley, M. Nei, and S. Kumar.** 2007. MEGA4: molecular evolutionary genetic analysis (MEGA) software version 4.0. Mol. Biol. Evol. **24**:1596–1599.
30. **Telenti, A., et al.** 1993. Rapid identification of mycobacteria to the species level by polymerase chain reaction and restriction enzyme analysis. J. Clin. Microbiol. **31**:175–178.
31. **Tsukamura, M., and H. Mikoshiba.** 1989. A taxonomic study on a mycobacterium which caused skin ulcer in a Japanese girl and resembled *Mycobacterium ulcerans*. Kekkaku **64**:691–697. (In Japanese.)
32. **Uganda Buruli Group.** 1971. Epidemiology of *Mycobacterium ulcerans* infection (Buruli ulcer) at Kinyara, Uganda. Trans. R. Soc. Trop. Med. Hyg. **65**:763–775.
33. **Wallace, R. J., Jr, D. R. Nash, L. C. Steele, and V. Steingrube.** 1986. Susceptibility testing of slowly growing mycobacteria by a microdilution MIC method with 7H9 broth. J. Clin. Microbiol. **24**:976–981.
34. **Walsh, D. S., F. Portaels, and W. M. Meyers.** 2011. Buruli ulcer: advances in understanding *Mycobacterium ulcerans* infection. Dermatol. Clin. **29**:1–8.
35. **Watanabe, T., et al.** 2010. Buruli ulcer caused by "*Mycobacterium ulcerans* subsp. *shinshuense*." Eur. J. Dermatol. **20**:809–810.
36. **World Health Organization.** October 2004. Provisional guidance on the role of specific antibiotics in the management of *Mycobacterium ulcerans* disease (Buruli ulcer). World Health Organization, Geneva, Switzerland. http://whqlibdoc.who.int/hq/2004/WHO_CD5_CPE_GBUI_2004.10.pdf..

JOURNAL OF BACTERIOLOGY, Oct. 2011, p. 5766–5774 Vol. 193, No. 20
0021-9193/11/$12.00 doi:10.1128/JB.05412-11

Structure and Host Recognition of Serotype 13 Glycopeptidolipid from *Mycobacterium intracellulare*▽†

Takashi Naka,[1,2]‡ Noboru Nakata,[3]‡ Shinji Maeda,[4]‡ Reina Yamamoto,[1,5] Matsumi Doe,[6] Seiko Mizuno,[1,5] Mamiko Niki,[1] Kazuo Kobayashi,[7] Hisashi Ogura,[1,8] Masahiko Makino,[3] and Nagatoshi Fujiwara[1]*

Departments of Bacteriology[1] and Virology,[8] Osaka City University Graduate School of Medicine, Osaka 545-8585, Japan; MBR Co. Ltd., Osaka 560-8552, Japan[2]; Department of Mycobacteriology, Leprosy Research Center, National Institute of Infectious Diseases, Tokyo 189-0002, Japan[3]; Molecular Epidemiology Division, Mycobacterium Reference Center, The Research Institute of Tuberculosis, Japan Anti-Tuberculosis Association, Tokyo 204-8533, Japan[4]; Department of Development Nourishment, Faculty of Human Development, Soai University, Osaka 559-0003, Japan[5]; Department of Chemistry, Graduate School of Science, Osaka City University, Osaka 558-8585, Japan[6]; and Department of Immunology, National Institute of Infectious Diseases, Tokyo 162-8640, Japan[7]

Received 31 May 2011/Accepted 31 July 2011

The *Mycobacterium avium-M. intracellulare* complex (MAIC) is divided into 28 serotypes by a species-specific glycopeptidolipid (GPL). Previously, we clarified the structures of serotype 7 GPL and two methyltransferase genes (*orfA* and *orfB*) in serotype 12 GPL. This study elucidated the chemical structure, biosynthesis gene, and host innate immune response of serotype 13 GPL. The oligosaccharide (OSE) structure of serotype 13 GPL was determined to be 4-2′-hydroxypropanoyl-amido-4,6-dideoxy-β-hexose-(1→3)-4-*O*-methyl-α-L-rhamnose-(1→3)-α-L-rhamnose-(1→3)-α-L-rhamnose-(1→2)-α-L-6-deoxy-talose by using chromatography, mass spectrometry, and nuclear magnetic resonance (NMR) analyses. The structure of the serotype 13 GPL was different from those of serotype 7 and 12 GPLs only in *O*-methylations. We found a relationship between the structure and biosynthesis gene cluster. *M. intracellulare* serotypes 12 and 13 have a 1.95-kb *orfA-orfB* gene responsible for 3-*O*-methylation at the terminal hexose, *orfB*, and 4-*O*-methylation at the rhamnose next to the terminal hexose, *orfA*. The serotype 13 *orfB* had a nonfunctional one-base missense mutation that modifies serotype 12 GPL to serotype 13 GPL. Moreover, the native serotype 13 GPL was multiacetylated and recognized via Toll-like receptor 2. The findings presented here imply that serotypes 7, 12, and 13 are phylogenetically related and confirm that acetylation of the GPL is necessary for host recognition. This study will promote better understanding of the structure-function relationships of GPLs and may open a new avenue for the prevention of MAIC infections.

The increase of drug-resistant mycobacteria and the number of immunocompromised hosts including the HIV epidemic are important problems. The *Mycobacterium avium-M. intracellulare* complex (MAIC) is distributed ubiquitously in the environment and is the most common isolate of nontuberculous mycobacteria, which are now one of the most important environmental pathogen-disseminated infectious agents in both immunocompromised and immunocompetent hosts (26, 31, 39).

The most characteristic feature of mycobacteria is richness in lipids. These hydrophobic cell wall components contribute to the surface properties and are considered to play important roles in their pathogenesis through the host immune responses (8, 17). MAIC expresses a glycopeptidolipid (GPL) as one of the representative lipid components. Structurally, the GPL is composed of two parts, a common tetrapeptido-amino alcohol core and a serotype-specific oligosaccharide (OSE) elongated from 6-deoxy-talose (6-d-Tal). D-Phenylalanine-D-*allo*-threonine-D-alanine-L-alaninol (D-Phe-D-*allo*-Thr-D-Ala-L-alaninol), which is modified with an amido-linked 3-hydroxy or 3-methoxy C_{26}-C_{34} fatty acid at the *N* terminus of D-Phe, and D-*allo*-Thr and terminal L-alaninol are further linked to a 6-d-Tal and 3,4-di-*O*-methyl rhamnose (3,4-di-*O*-Me-Rha), respectively. This portion is called the serotype-nonspecific GPL (apolar GPL). Serotype-specific GPLs (polar GPLs) are produced by extending individual OSE residues from the 6-d-Tal. MAIC species are divided into 28 serotypes by serological reaction and distinctive patterns of polar GPLs on thin-layer chromatography (TLC) (7, 38). The GPL is considered to play crucial roles in the physiology of the bacteria and the host responses to MAIC infection. Several biological and immunological functions of GPLs have been reported (9, 34), but the roles of GPLs are not fully elucidated. Recently, several genes involved in GPL biosynthesis have been characterized (10, 29). To better understand the biological functions and significance of GPLs, we need to clarify the structure and biosynthetic pathways of GPLs.

The chemical structures of only 16 GPLs have been defined (9). Recently, we determined the structures of the serotype 7 and 16 GPLs and identified the gene clusters completing the OSE biosynthesis (13, 14). In addition, two methyltransferase genes of serotype 7- and 12-specific GPL biosynthesis were

* Corresponding author. Mailing address: Department of Bacteriology, Osaka City University Graduate School of Medicine, 1-4-3 Asahi-machi, Abeno-ku, Osaka 545-8585, Japan. Phone: 81 6 6645 3746. Fax: 81 6 6645 3747. E-mail: fujiwara@med.osaka-cu.ac.jp.

† Supplemental material for this article may be found at http://jb.asm.org/.

‡ These authors contributed equally to this work.

▽ Published ahead of print on 19 August 2011.

characterized (30). In this process, we found that the structure of the serotype 13 GPL is close to that of the serotype 7 and 12 GPLs. In epidemiological serotyping, Tsang et al. (37) showed that clinical isolates of serotypes 7, 12, and 13 were found in around 10% of non-AIDS patients. However, it was difficult to distinguish serotypes 7, 12, and 13 by only serological and chromatographic techniques because of their structural similarity. The phylogeny of some MAIC strains based on GPL biosynthesis genes has been reported (23). In this study, the complete structure of the serotype 13 GPL was determined, and the genetic relationship between the serotype 7, 12, and 13 GPL biosynthesis was clarified. Moreover, the host innate immune recognition of antigenic serotype 13 GPL and the importance of structural modification were shown. We discuss the phylogeny of MAIC strains on the basis of these GPL biosynthesis genes and the relationship between GPL structure and immunogenicity.

MATERIALS AND METHODS

Bacterial strains and preparation of GPL. *M. intracellulare* serotype 13 (ATCC 35769, ATCC 25122), serotype 7 (ATCC 35847), and serotype 12 (ATCC 35762) strains were purchased from the American Type Culture Collection (Manassas, VA). The GPL preparation was performed as described previously (14, 18). Each strain of *M. intracellulare* was grown on Middlebrook 7H11 agar (Difco Laboratories, Detroit, MI) with 0.5% glycerol and 10% Middlebrook oleic acid-albumin-dextrose-catalase (OADC) enrichment (Difco) at 37°C for 2 to 3 weeks. The heat-killed bacteria were sonicated, and crude lipids were extracted with chloroform-methanol (2:1 [vol/vol]). The crude lipids were hydrolyzed with 0.2 N sodium hydroxide in methanol at 37°C for 2 h, followed by neutralization with 6 N hydrochloric acid. Alkaline-stable lipids were partitioned by a two-layer system with chloroform-methanol (2:1 [vol/vol]) and water. The organic phase was evaporated and precipitated with acetone to remove any acetone-insoluble components. The supernatant was washed (chloroform-methanol, 95:5 [vol/vol]) and eluted (chloroform-methanol, 1:1 [vol/vol]) with a Sep-Pak silica cartridge (Waters Corporation, Milford, MA) for partial purification. The GPL was completely purified by preparative TLC of Silicagel G (Uniplate; 20 by 20 cm, 250 μm; Analtech, Inc., Newark, DE). The TLC plate was developed with chloroform-methanol-water (65:25:4 and 60:16:2 [vol/vol/vol]), until a single spot was obtained. The TLC plate was sprayed with 20% sulfuric acid in ethanol and was charred at 180°C for 3 min. The GPL was detected as a brownish-yellow spot. To recover the GPL, the TLC plate was exposed to iodine vapor, and the GPL spot was marked. The silica gels of the GPL spot were scraped off, and the GPL was eluted with chloroform-methanol (2:1 [vol/vol]). The native GPL was purified by the same method as the alkaline-stable GPL, omitting the hydrolysis with 0.2 N sodium hydroxide.

Preparation of OSE moiety. β-Elimination of the GPL was performed with alkaline borohydride, and the OSE elongated from D-*allo*-Thr was released (14, 18). The GPL was stirred in a solution of equal volumes of ethanol and 10 mg/ml sodium borodeuteride in 0.5 N sodium hydroxide at 60°C for 16 h. The reaction mixture was decationized with Dowex 50W X8 beads (Dow Chemical Company, Midland, MI) and evaporated under nitrogen to remove boric acid. After partition into two layers of chloroform-methanol (2:1 [vol/vol]) and water, the upper aqueous phase was recovered and evaporated, and the OSE was purified as an oligoglycosyl alditol.

MALDI-TOF MS and MALDI-TOF MS/MS. The molecular species of the intact GPL was determined by the matrix-assisted laser desorption ionization–time of flight mass spectrometry (MALDI-TOF MS) with an Ultraflex II (Bruker Daltonics, Billerica, MA). One microgram of the GPL-dissolved chloroform-methanol (2:1 [vol/vol]) was applied to the target plate, and 1 μl of 10 mg/ml 2,5-dihydroxybenzoic acid in chloroform-methanol (1:1 [vol/vol]) was added as a matrix. The intact GPL was analyzed in the Reflectron mode with an accelerating voltage operating in positive mode at 20 kV (4). Then, the fragment pattern of the OSE was analyzed with the MALDI-TOF MS/MS mode. The OSE and 10 mg/ml 2,5-dihydroxybenzoic acid was dissolved in ethanol-water (3:7 [vol/vol]) and applied to the target plate according to the method for intact GPL.

GC/MS of carbohydrates. To determine the glycosyl composition and linkage position, gas chromatography/mass spectrometry (GC/MS) of partially methylated alditol acetate derivatives was performed. Perdeuteromethylation was conducted by the modified procedure of Hakomori (14, 15). The OSE was dissolved with a mixture of dimethyl sulfoxide and sodium hydroxide, followed by the addition of deuteromethyl iodide. After stirring at room temperature for 15 min, the reaction mixture was separated by a two-layer system of water and chloroform. The chloroform-containing perdeuteromethylated OSE layer was collected, washed with water two times, and evaporated completely. Partially deuteromethylated alditol acetate derivatives were prepared from perdeuteromethylated OSE by hydrolysis with 2 N trifluoroacetic acid at 120°C for 2 h, reduction with 10 mg/ml sodium borodeuteride at 25°C for 2 h, and acetylation with acetic anhydride at 100°C for 1 h (14, 19). GC/MS was performed using a benchtop ion trap mass spectrometer (GCMS-QP2010 Plus; Shimadzu Corp., Kyoto, Japan) equipped with a fused capillary column (SP-2380 and Equity-1; 30 m, 0.25-mm inner diameter [ID]; Supelco, Bellefonte, PA). Helium was used

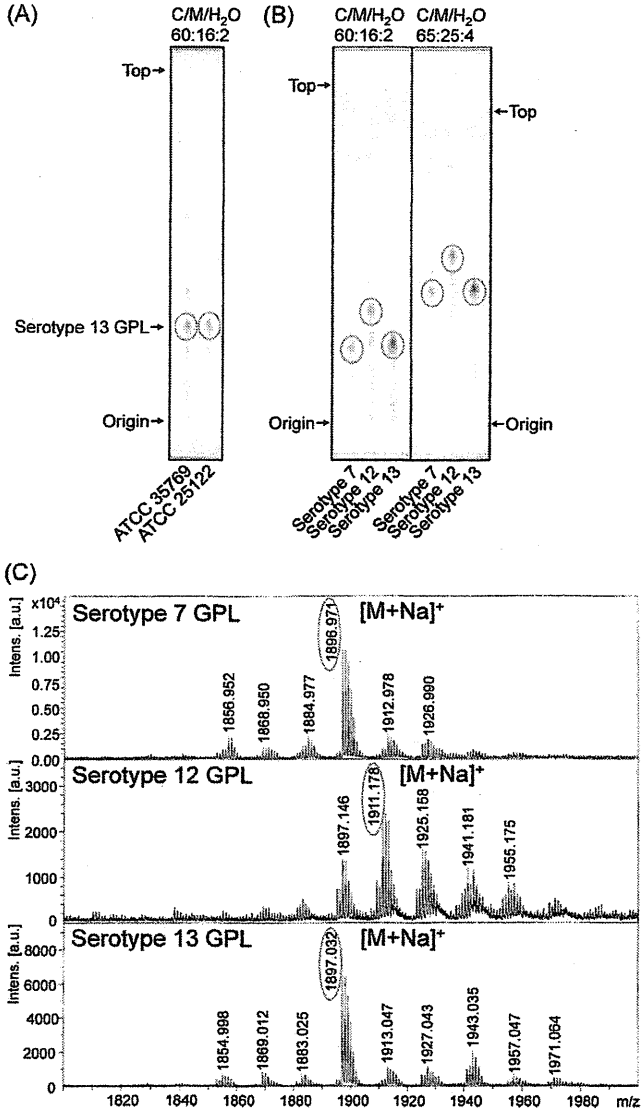

FIG. 1. TLC patterns and MALDI-TOF MS spectra of serotype 7, 12, and 13 GPLs. (A and B) The alkaline-stable lipids derived from *M. intracellulare* serotype 13 ATCC 35769 and ATCC 25122 (A) and the purified serotype 7, 12, and 13 GPLs (B) were developed on TLC plates with solvent systems of chloroform-methanol-water (60:16:2 and 65:25:4 [vol/vol/vol]). (C) The MALDI-TOF MS spectra of serotype 7, 12, and 13 GPLs were acquired using 10 mg/ml 2,5-dihydroxybenzoic acid in chloroform-methanol (1:1 [vol/vol]) as a matrix, and the molecular ions were detected as $[M+Na]^+$ in positive mode. Intens., intensity; a.u., arbitrary units.

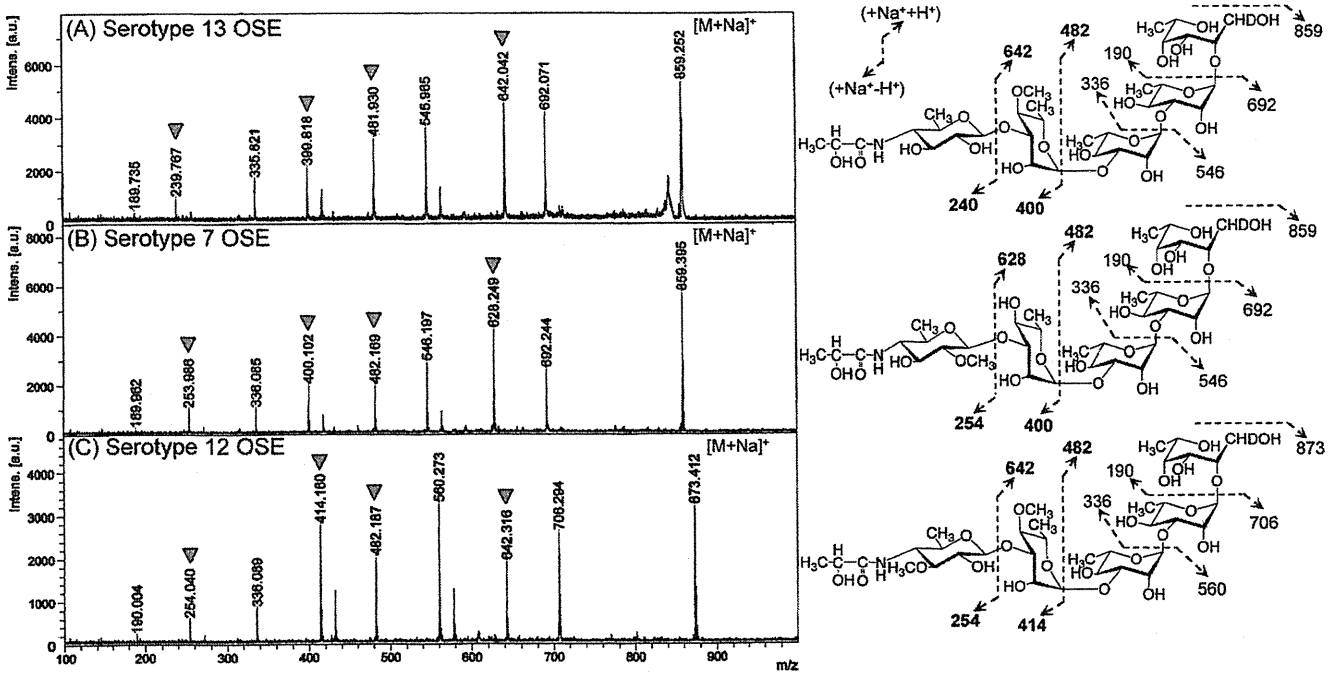

FIG. 2. MALDI-TOF MS/MS spectra of serotype 13, 7, and 12 OSEs (A, B, and C, respectively). The fragment ions by each glycosyl cleavage were detected, and the assigned fragment patterns are illustrated. Arrowheads indicate the characteristic mass numbers of the serotype 13, 7, and 12 OSEs. The matrix was 10 mg/ml 2,5-dihydroxybenzoic acid in ethanol-water (3:7 [vol/vol]), and it was performed in the MS/MS mode. Intens., intensity; a.u., arbitrary units.

as the carrier gas, and the flow rate was 1 ml/min. The temperature program for alditol acetate derivatives was started at 60°C, increased 40°C/min to 220°C, and held for 15 min, followed by an increase of 10°C/min to 260°C and holding for 10 min. The molecular separator and ion source energies were 70 eV, and the accelerating voltage was 8 kV.

NMR of GPL. The OSE was dissolved in deuterium oxide. To define the anomeric configurations of each glycosyl residue, ^{1}H and ^{13}C nuclear magnetic resonance (NMR) was employed. Both homonuclear correlation spectrometry (COSY) and ^{1}H-detected [^{1}H, ^{13}C] heteronuclear multiple-quantum correlation (HMQC) were recorded with a Bruker AVANCE-600 (Bruker BioSpin Corp. Billerica, MA), as described previously (14, 18). Ten microliters of acetone was added to the sample, and its chemical shift values, 2.04 ppm (proton) and 29.8 ppm (carbon), were used as internal controls.

Sequencing of *orfA-orfB* region of *M. intracellulare* serotype 13. PCR was used to amplify the *orfA-orfB* region (30) of *M. intracellulare* serotype 13 (ATCC 35769 and ATCC 25122), using primers *orfA*-F (5′-GCGGATCCAGTGTGCAGACG AGCGGAACT-3′), *orfA*-R (5′-GCGAATTCTTATCGAGAAAAAATAAAA G-3′), *orfB*-F (5′-GCGGATCCACTGCTAGACT CCGCCACCAT-3′), and *orfB*-R (5′-GCGAATTCCTACACCTTCACGGCGAGTC-3′). The amplified fragment was sequenced using a BigDye Terminator cycle sequencing kit, version 3.1 (Applied Biosystems, Foster City, CA), and a sequence analyzer (ABI3130xl; Applied Biosystems).

Transformation of *M. intracellulare* serotype 13 strain with serotype 12 *orfB*. The *orfB* fragments from serotype 12 (sero12-*orfB*) and serotype 13 (sero13-*orfB*) strains were amplified and cloned into pVV16, an expression plasmid vector for mycobacteria, downstream of the hsp60 promoter. *M. intracellulare* serotype 13 ATCC 35769 was transformed with pVV16-sero12-*orfB* and pVV16-sero13-*orfB* by electroporation, and hygromycin- and kanamycin-resistant colonies were isolated. Alkaline-stable lipids were prepared from heat-killed bacteria, and productive GPLs were identified by TLC, MALDI-TOF MS, MALDI-TOF MS/MS, and GC/MS.

Host recognition of native and alkaline-treated serotype 13 GPLs. The host recognition of GPLs was estimated by activations of HEK-blue-2 and -4 cells (InvivoGen, San Diego, CA). HEK-blue-2 and -4 cells are HEK293 cells stably transfected with multiple genes for recognition of Toll-like receptor 2 (TLR2) and TLR4 (including the coreceptors MD2 and CD14). In addition, HEK-blue-2 and -4 cells stably express an optimized alkaline phosphatase gene engineered to be secreted (sAP) and placed under the control of a promoter inducible by several transcription factors, such as NF-κB and alkaline phosphatase-1. HEK-blue-2 and -4 cells were seeded at a concentration of 2×10^5 cells/ml in 96-well flat-bottom tissue culture plates and incubated with Dulbecco's modified Eagle's medium (DMEM) containing 10% fetal bovine serum (FBS) at 37°C in an atmosphere of 5% CO_2 for 3 days. The adherent HEK-blue-2 and -4 cells were stimulated by native and alkaline-treated serotype 13 GPLs. After 24 h of incubation, NF-κB activation was assayed by the levels of sAP in the supernatant. The sAP was measured in duplicate using QUANTI-Blue (InvivoGen) according to the manufacturer's instructions. As positive controls, we used lipopolysaccharide (LPS) from *Escherichia coli* 055:B5 (Sigma-Aldrich, St. Louis, MO) for TLR4 and Pam3CSK4 (InvivoGen) for TLR2. Two independent experiments were performed.

Nucleotide sequence accession number. The nucleotide sequence reported here has been deposited in the NCBI GenBank database under accession number AB557690.

RESULTS

Purification and molecular weight of intact GPL. The serotype 13 GPLs from *M. intracellulare* ATCC 35769 and 25122 were detected as spots on TLC plates and showed the same R_f value (Fig. 1A). Because serotype 13 GPL was predicted to be very close structurally to the serotype 7 and 12 GPLs, the R_f values were compared on TLC plates developed with two different chloroform-methanol-water solvent systems (65:25:4 and 60:16:2 [vol/vol/vol]), respectively. Interestingly, the R_f value of the serotype 13 GPL was lower than that of the serotype 12 GPL and almost the same as that of the serotype 7 GPL in both developing systems (Fig. 1B). The intact molecular weight of each GPL was determined. The MALDI-TOF MS spectrum of the serotype 13 GPL showed *m/z* 1,897 for $[M+Na]^+$ as the main molecular ion in positive mode (Fig.

1C). This mass number is identical to that of the serotype 7 GPL ($[M+Na]^+$: 1,897) and 14 atomic mass units lower than that of the serotype 12 GPL ($[M+Na]^+$: 1,911).

Glycosyl sequence of serotype 13 OSE. To determine the glycosyl sequence of the OSE, MALDI-TOF MS/MS of the oligoglycosyl alditol from serotype 13 OSE was performed. The spectrum afforded the molecular ion $[M+Na]^+$ at *m/z* 859, together with the characteristic mass increments in the series of glycosyloxonium ions formed on fragmentation at *m/z* 240, 400, 546, and 692 from the *N*-acylated Hex to 6-d-Tal, and at *m/z* 190, 336, 482, and 642 from 6-d-Tal to *N*-acylated Hex (Fig. 2A). In comparison, the fragment patterns of the cleaved terminal *N*-acylated Hex of the OSEs were *m/z* 254 and 628 in serotype 7 and *m/z* 254 and 642 in serotype 12, and those next to the terminal Hex were *m/z* 400 and 482 in serotype 7 and *m/z* 414 and 482 in serotype 12 (Fig. 2B and C). Together with the intact molecular weight of each GPL (Fig. 1B), these results strongly implied that serotype 13 GPL has no *O*-methyl group in the terminal *N*-acylated Hex but does have an *O*-methyl group added to the Rha next to the terminal Hex.

Carbohydrate composition and linkage analyses. GC/MS analysis of the perdeuteromethylated alditol acetate derivative from serotype 13 OSE was performed to determine the glycosyl composition. The total ion chromatography (TIC) of the GC/MS spectrum of serotype 13 GPL derivatives was compared to those of serotype 7 and 12 GPL derivatives (Fig. 3A). Previous reports showed that the carbohydrate compositions of the serotype 7 GPL were 6-d-Tal, Rha, and 4-2′-hydroxypropanoyl-amido-3,6-dideoxy-2-*O*-Me-Hex, and those of the serotype 12 GPL were 6-d-Tal, Rha, 4-*O*-Me-Rha, and 4-2′-hydroxypropanoyl-amido-3,6-dideoxy-3-*O*-Me-Hex (5, 13). Comparison of the retention times and mass spectra of GC/MS determined that serotype 13 GPL was composed of 6-d-Tal, Rha, 4-*O*-Me-Rha, and another terminal *N*-acylated Hex. As shown in Fig. 3B, the perdeuteromethylated alditol acetate derivative of the terminal *N*-acylated Hex was assigned to 2,3-di-*O*-deuteromethyl-1,5-di-*O*-acetyl-4-2′-*O*-deuteromethyl-propanoyl-deuteromethylamido-4,6-dideoxy-hexitol from the fragment pattern (*m/z* 62, 108, 121, 168, 209, 222, 269, and 303). These results confirmed that the *O*-methyl group was deleted from the terminal *N*-acylated Hex and added to the C-4 position at Rha next to the terminal Hex. Taken together, these results established the sequence and linkage arrangement of 4-2′-hydroxypropanoyl-amido-4,6-dideoxy-Hex-(1→3)-4-*O*-Me-Rha-(1→3)-L-Rha-(1→3)-L-Rha-(1→2)-6-d-Tal exclusively.

NMR analysis of serotype 13 OSE. The ^1H NMR and ^1H-^1H homonuclear COSY analyses of the OSE derived from the serotype 13 GPL revealed four distinct anomeric protons with corresponding H1-H2 cross-peaks in the low-field region at δ4.88, 4.71, 4.97 (J_{1-2} = 1 to 2 Hz, indicative of α-anomers), and 4.52 (a doublet, J_{1-2} = 7.9 Hz, indicative of a β-hexosyl unit). When further analyzed by ^1H-detected [^1H-^{13}C] two-dimensional HMQC, the anomeric protons resonating at δ4.88, 4.71, 4.97, and 4.52 had C-1s resonating at δ102.10, 93.50, 94.00, and 103.40, respectively. The J_{CH} values for each of these protons were calculated to be 170, 170, 171, and 161 Hz by measurement of the inverse-detection nondecoupled two-dimensional HMQC (see Fig. S1 and Table S1 in the supplemental material). It was concluded that two Rha and 4-*O*-Me Rha were α-anomers and that the terminal *N*-acylated Hex was a β configuration.

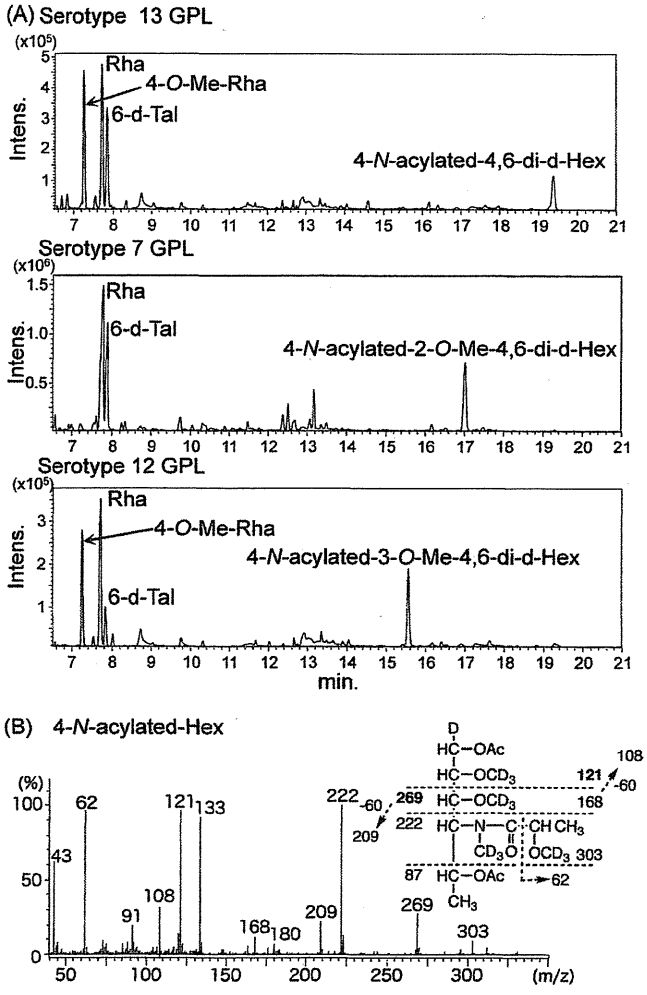

FIG. 3. Assignment of glycosyl composition of OSEs in serotype 13 GPL. (A) Total ion chromatogram of the alditol acetate derivatives from serotype 13 compared to those of serotype 7 and 12 GPLs. A fused SP-2380 capillary column was used as the GC column. The temperature program for alditol acetate derivatives was started at 60°C, increased to 40°C/min to 220°C, and held for 15 min, followed by an increase of 10°C/min to 260°C and holding for 10 min. (B) GC/MS spectrum of the perdeuteromethylated alditol acetate derivative from the terminal Hex in serotype 13 GPL. The pattern of prominent fragment ions is illustrated. A fused Equity-1 capillary column was used as the GC column. Ac, CH_3CO.

Nucleotide sequence of *orfA-orfB* region of *M. intracellulare* serotype 13. The present study demonstrated that the difference between the chemical structures of the serotype 13 GPL and serotype 7 and 12 GPLs was whether the *O*-methyl group in the terminal *N*-acylated Hex and the next Rha were present or not. We confirmed the genetic basis of these *O*-methylations. Our previous study clarified three unique open reading frames (ORFs) for methyltransferase, named *orf2*, derived from *M. intracellulare* serotype 7, and *orfA* and *orfB*, from *M. intracellulare* serotype 12 (13, 30). *orfA* and *orfB* in *M. intracellulare* serotype 12 are responsible for 4-*O*-methylation of the Rha next to the terminal Hex and 3-*O*-methylation of the

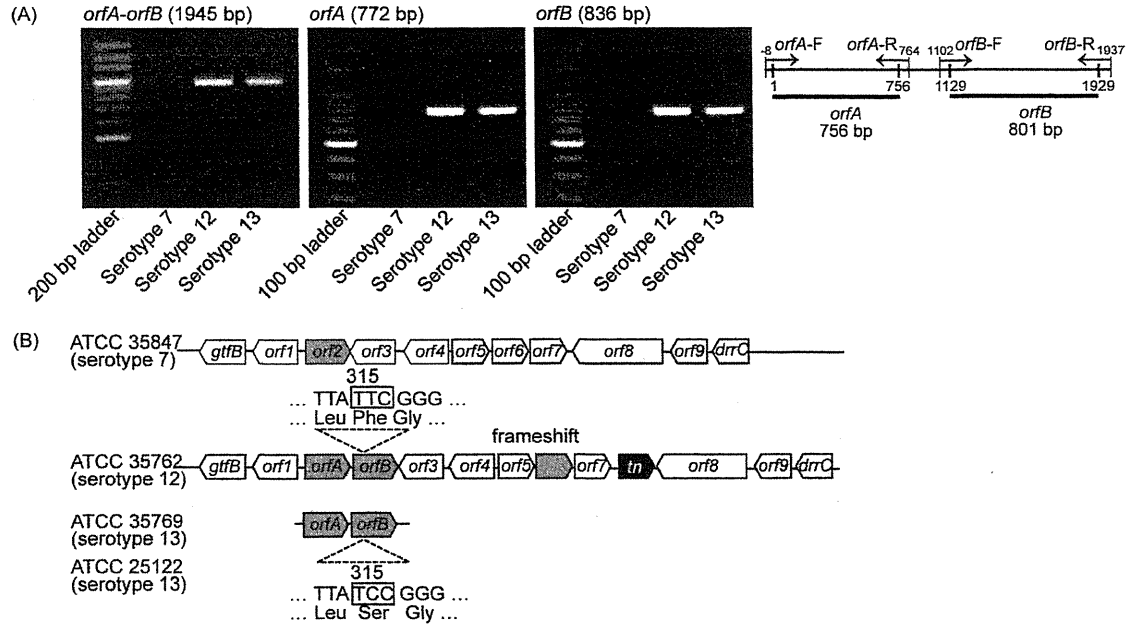

FIG. 4. Detection of *orfA-orfB* regions and comparison of genetic maps of GPL biosynthetic cluster. (A) PCR was performed to amplify the *orfA-orfB* regions of *M. intracellulare* serotype 7, 12, and 13 strains. The primers and the amplified regions are indicated. (B) *M. intracellulare* serotype 7 ATCC 35847 and serotype 12 ATCC 35762 were sequenced in our previous work (13, 30). *M. intracellulare* serotype 13 ATCC 35769 and ATCC 25122 were sequenced in this study. The missense mutation of *orfA-orfB* regions is indicated.

terminal Hex, respectively. Therefore, we examined whether or not *M. intracellulare* serotype 13 has these ORFs. First, comparison of the *gtfB-drrC* gene cluster in *M. intracellulare* serotype 7 and 12 strains implied that *orf2* in *M. intracellulare* serotype 7 replaced *orfA-orfB* in *M. intracellulare* serotype 12. We amplified the *orfA-orfB* in the genomic DNA from *M. intracellulare* serotypes 7, 12, and 13 (Fig. 4A). Interestingly, *M. intracellulare* serotype 13 had the same-sized DNA fragment of the *orfA-orfB* region, and the nucleotide sequences were determined. The 1.95-kb *orfA-orfB* regions of the two serotype 13 strains had complete identity and showed only one nucleotide substitution from that of serotype 12: codon 105, TTC, of the *orfB* in serotype 12 was replaced by codon TCC in serotype 13 (Fig. 4B). This missense mutation induced a single amino acid substitution from Phe to Ser and implied the loss of the *orfB* activity for *O*-methylation.

Expression of sero12-*orfB* and sero13-*orfB* in *M. intracellulare* serotype 13. To test the functional activity of *orfB* in *M. intracellulare* serotypes 12 and 13, the sero12-*orfB* and sero13-*orfB* genes were introduced into the *M. intracellulare* serotype 13 strain. The 0.84-kb sero12-*orfB* and sero13-*orfB* were amplified and cloned into a pVV16 vector, and *M. intracellulare* serotype 13 ATCC 35769 was transformed with the resulting plasmids and the pVV16 vector. The alkaline-stable lipids derived from the transformants were developed on TLC plates, and the productive GPLs were compared to the spots of serotype 7, 12, and 13 GPLs (Fig. 5A). Both R_f values of the GPLs produced in the transformants with the pVV16 vector and sero13-*orfB* were identical to that of the serotype 13 GPL. However, the R_f value of the GPL produced in the transformant with sero12-*orfB* was the same as that of serotype 12 GPL. By MALDI-TOF MS, the main molecular weights of the GPLs produced in the transformants with sero12-*orfB*, sero13-*orfB*, and the pVV16 vector were detected as *m/z* 1,911, 1,897, and 1,897, respectively, for $[M+Na]^+$ (data not shown). The fragment ions of the related glycosyl cleavage in the OSEs were analyzed by using MALDI-TOF MS/MS, and the glycosyl compositions were determined. The fragment ions of the OSEs in the pVV16 vector and sero13-*orfB* showed the same pattern as serotype 13 GPL, indicating that overexpression of sero13-*orfB* in the serotype 13 strain was not affected (Fig. 2A and 5B). The fragment ions of the OSE in sero12-*orfB*, i.e., *m/z* 254 and 414, were different from those of the OSE in sero13-*orfB*, i.e., *m/z* 240 and 400, respectively (Fig. 5B). The GC/MS spectrum of the perdeuteromethylated alditol acetate derivative of the terminal *N*-acylated Hex from sero12-*orfB* was assigned to 2-*O*-deuteromethyl-1,5-di-*O*-acetyl-4-2′-*O*-deuteromethyl-propanoyl-deuteromethylamido-4,6-dideoxy-3-*O*-methyl-hexitol from the fragment pattern (*m/z* 62, 105, 121, 165, 206, 222, 266, and 300) (Fig. 5C), which was identical to that of the serotype 12 GPL. These results demonstrated that the serotype 13 transformant with sero12-*orfB* but not sero13-*orfB* had an added *O*-methyl group at the C-3 position in the terminal Hex and that the productive GPL was completely changed from serotype 13 to serotype 12. In addition, we confirmed that the plasmid-deleted C-terminal 40-base region of sero12-*orfB* was completely functional and that sero12-*orfB* worked in the serotype 7 transformant. Taken together, these results indicated that sero13-*orfB* was inactivated by the missense mutation at codon 105 and that the serotype 13 GPL lacked *O*-methylation at the C-3 position of the terminal Hex.

Native conformation of serotype 13 GPL and host response. The native serotype 13 GPL was purified without alkaline treatment. The native serotype 13 GPLs were detected on TLC

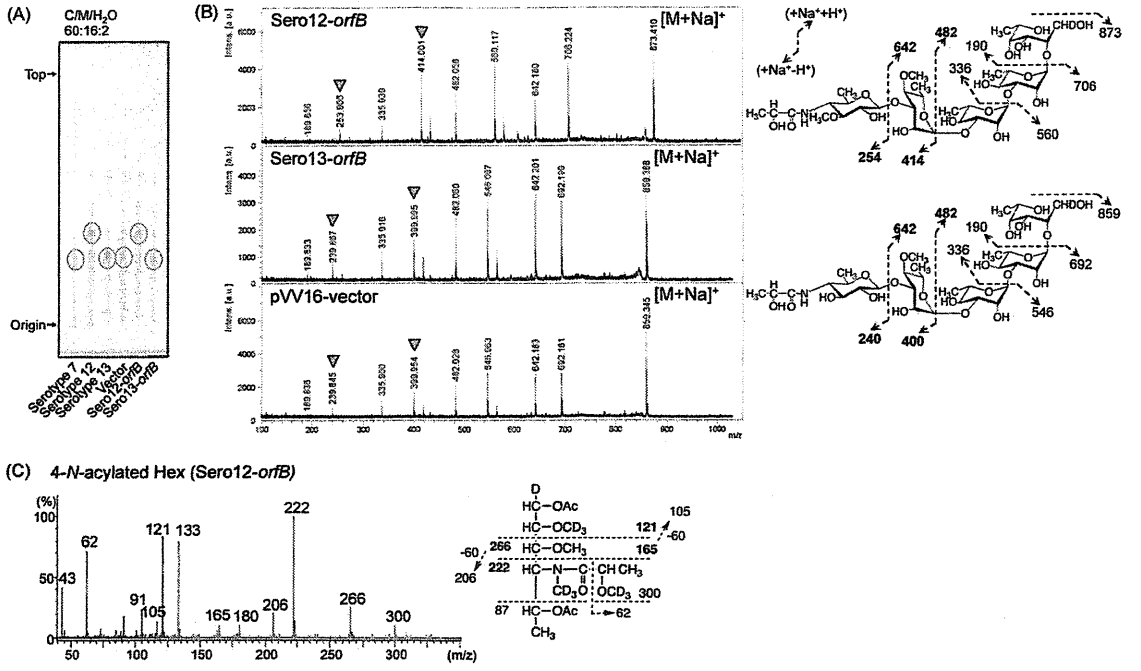

FIG. 5. The productive GPLs in transformants of *M. intracellulare* serotype 13 with sero12-*orfB* or sero13-*orfB*. (A) TLC patterns of the alkaline-stable lipids derived from *M. intracellulare* serotypes 7, 12, and 13 and serotype 13 transformants (ATCC 35769) with the pVV16-vector, sero12-*orfB*, and sero13-*orfB* from left to right, developing with a solvent system of chloroform-methanol-water (60:16:2 [vol/vol/vol]). (B) MALDI-TOF MS/MS spectra of OSEs derived from the productive GPLs in transformants of *M. intracellulare* serotype 13 with sero12-*orfB*, sero13-*orfB*, and the pVV16 vector. The replaced mass numbers are indicated by arrowheads. (C) GC/MS spectrum of the perdeuteromethylated alditol acetate derivative of the terminal *N*-acylated Hex from serotype 13 transformant with sero12-*orfB*. The MALDI TOF MS/MS and GC/MS conditions are described in the legends for Fig. 2 and 3. Ac, CH_3CO.

plates as three major spots that expanded broadly and had R_f values different from that of the alkaline-treated serotype 13 GPL. These spots were converged into one spot by alkaline treatment (Fig. 6A). It was reported that some positions of OSE in GPLs are acetylated in nature (27). The molecular weights of these three spots were checked by MALDI-TOF MS. The mass numbers of *m/z* 1,983, 2,025, and 2,067 for $[M+Na]^+$ caused the 2- to 4-unit increases of *m/z* 42 (addition of acetylations) and the modification to saturated alkyl group, compared to *m/z* 1,897 of the alkaline-treated serotype 13 GPL, implying that native GPLs were modified by several *O*-acetylations in the OSE portion and that alkaline treatment removed the acetylated groups (Fig. 6B). In addition, several peaks at intervals of 14 atomic mass units were caused by an alkyl group, indicating that the fatty acids of the core portion were variable and that the molecular species were heterogeneous.

To clarify the host recognitions of serotype 13 GPL via TLRs, we stimulated HEK-blue-2 and -4 cells with native and alkaline-treated serotype 13 GPLs. The native serotype 13 GPL significantly activated HEK-blue-2 cells in a dose-dependent manner, but HEK-blue-4 cells did not respond. The alkaline-treated serotype 13 GPL without *O*-acetylation did not activate either HEK-blue-2 or -4 cells. Reacetylated alkaline-treated serotype 13 GPLs with *O*-acetyl groups substituted for all hydroxy groups of OSE activated HEK-blue-2 cells, although the level of activation was less than that of the native form (Fig. 6C). Moreover, we confirmed that only the native serotype 13 GPL stimulated mouse bone marrow-derived macrophages via TLR2 by using C57BL/6 and TLR2 knockout mice (see Fig. S2 in the supplemental material).

DISCUSSION

The structural heterogeneity of the GPLs in MAIC species is reflected in their morphology, virulence, and pathogenicity (2, 3, 24) and may be meaningful in phylogenetic classification. Actually, epidemiological studies show that the isolates of MAIC serotypes from patients are heterogeneous and important for assessing the prognosis of pulmonary MAIC disease (25, 37). Chatterjee and Khoo (9) proposed grouping the three types of GPLs by OSE structure, and the group 2 GPLs included the serotype 12, 17, and 19 strains. The serotype 7 and 16 GPLs determined in our previous studies also belong to the group 2 GPLs (13, 14). The group 2 GPLs have in common 6-d-Tal-Rha-Rha and serotype-individual sugars elongated from the second Rha. In addition, except for the serotype 19 GPL, group 2 GPLs carry an unusual substituent, *N*-acylated amido sugar, as the terminal Hex. Aspinall et al. (1) mentioned that the terminal sugar residue of serotype 12 GPL is a derivative of viosamine (4-amino-4,6-dideoxyglucose). The structural difference between serotype 7 and 12 GPLs in group 2 was due to the functions of three methyltransferase genes, *orf2*, *orfA*, and *orfB* (13, 30). In this study, we found that the serotype 13 GPL was structurally very close to those of serotypes 7 and 12, and we determined the novel structure of

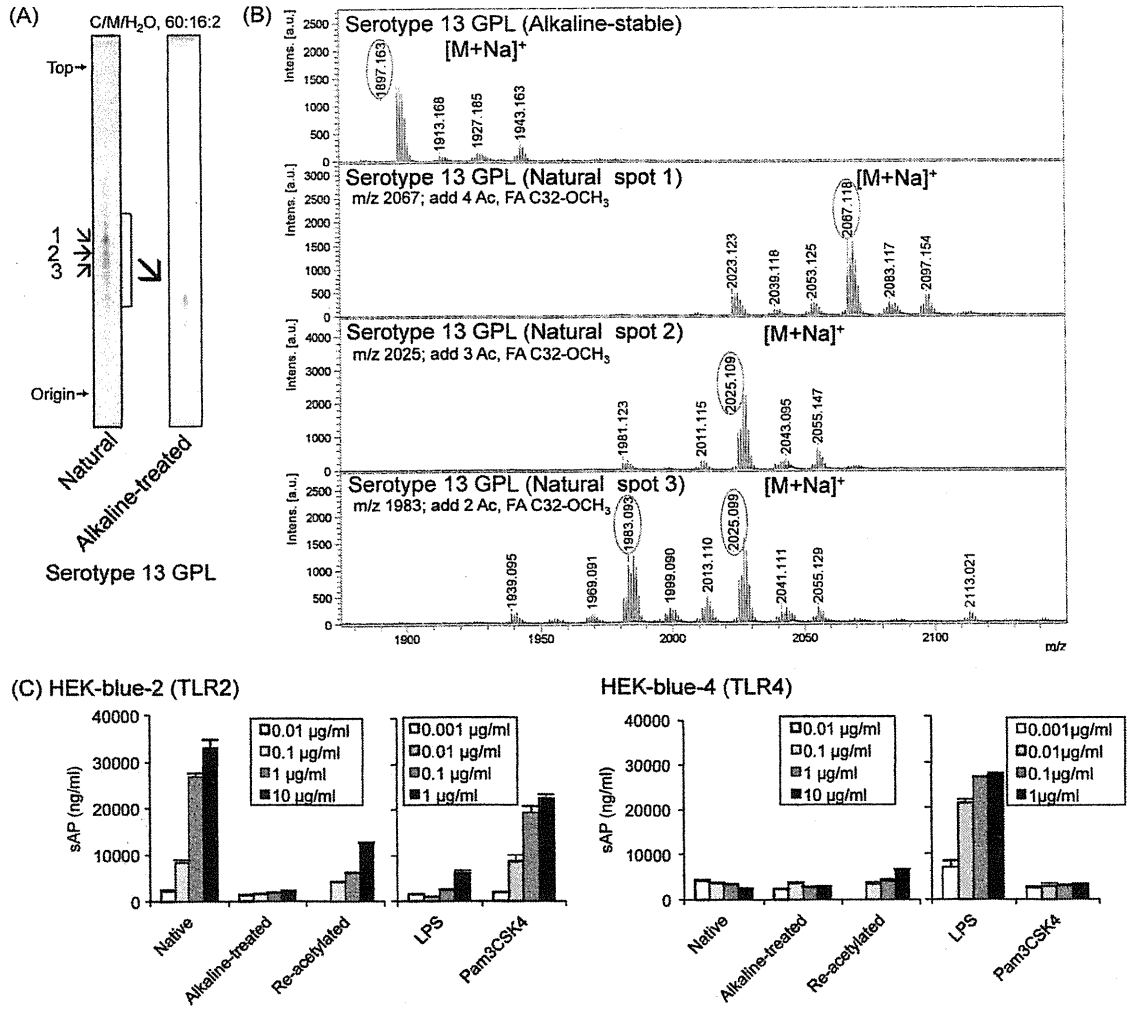

FIG. 6. TLC patterns, MALDI-TOF MS spectra, and TLR recognition of the native and alkaline-treated serotype 13 GPL. (A) The TLC plate was developed with a solvent system of chloroform-methanol-water (60:16:2 [vol/vol/vol]). Three major spots of native GPL are indicated by the numbers from top to bottom. (B) The major spots were purified and their molecular ions were measured by MALDI-TOF MS. The condition is described in the legend for Fig. 1. (C) HEK-blue-2 and -4 cells (2×10^5 cells/ml) were stimulated with native, alkaline-treated, and reacetylated serotype 13 GPLs. After 24 h of incubation, NF-κB activation was assessed by measuring the levels of secreted alkaline phosphatase (sAP) in the supernatant by using QUANTI-Blue. The data are means ± standard deviations (SD) for two experiments done in duplicate.

the serotype 13 GPL to be 4-2′-hydroxypropanoyl-amido-4,6-dideoxy-β-hexose-(1→3)-4-*O*-methyl-α-L-rhamnose-(1→3)-α-L-rhamnose-(1→3)-α-L-rhamnose-(1→2)-α-L-6-deoxy-talose. This result clarified that the serotype 13 GPL is structurally different from the serotype 7 and 12 GPLs in the *O*-methylations of the terminal *N*-acylated Hex and Rha next to the terminal Hex. Serotype 13 GPL lacked the *O*-methyl group in the terminal *N*-acylated Hex, although serotype 7 and 12 GPLs had one at the C-2 and C-3 positions, respectively. The composition and position of the *N*-acyl group at the terminal Hex were completely identical in these three GPLs. At the Rha next to the terminal Hex, serotype 12 and 13 GPLs have an *O*-methyl group at the C-4 position, and this modification is present in all group 2 GPLs except for the serotype 7 GPL, suggesting that this methyl group may play a role in MAIC physiology and virulence. These results also implied that *M. intracellulare* serotypes 7, 12, and 13 are very close phylogenetically.

We investigated the relationship between the structure and biosynthetic pathway and tried to verify the phylogenetic classification of serotypes 7, 12, and 13 by genetic analysis of GPL biosynthesis. We previously reported the nucleotide sequences of the *gtfB-drrC* region, which completely determine each serotype-specific GPL in serotypes 7 and 12 (13, 30), and found the sequence of the serotype 13 gene cluster (unpublished data). The genetic organizations of the *gtfB-drrC* regions in serotype 7, 12, and 13 gene clusters closely resemble each other. Seven common ORFs are conserved in *gtfB-drrC* clusters, suggesting that these three serotypes diverged from a common ancestor. The *orfA-orfB* region in serotypes 12 and 13 replaced *orf2* in serotype 7. Only one nucleotide substitution was found in the 1.95-kb segment in *orfA-orfB* of serotypes 12

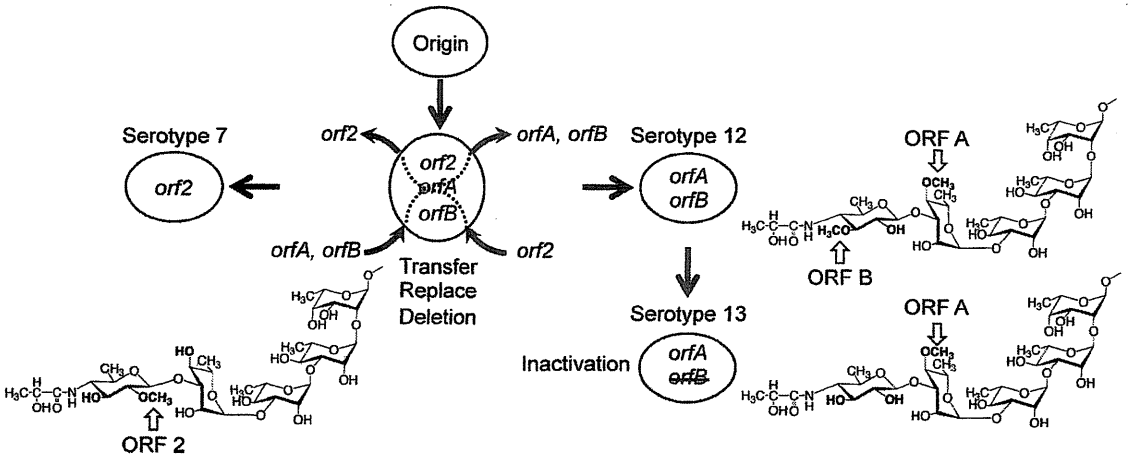

FIG. 7. Scheme of the relationship between GPL biosynthesis ORFs encoded the methyltransferases and their structures.

and 13, and *orfB* in serotype 13 was inactivated. In general, it is unusual for an ORF inactivated by a missense mutation to remain in the genome because it is a burden for the bacterium to transcribe and translate an inactivated ORF. Thus, the *M. intracellulare* serotype 13 strain must have diverged from an *M. intracellulare* serotype 12 organism recently. Serotype 13 GPL also has 4-*O*-Me-Rha. *orfA* is responsible for this methylation. In previous studies, we demonstrated that the *orfB* activity had incapacitated the *orf2* activity, which synthesizes an *O*-methyl group at the C-2 position of the terminal Hex of *M. intracellulare* serotype 7. We also showed that the *orf2* activity was independent of *orfA* activity in *M. intracellulare* serotype 12 (30). The relation of methyltransferases, *orfA*, *orfB*, and *orf2* is summarized in Fig. 7.

GPLs are correlated with colony morphology, sliding motility, biofilm formation, immune modulation, and virulence (2, 3, 16, 34). GPLs have several significant features. They are produced in MAIC species and absent from *Mycobacterium tuberculosis*, making it possible to distinguish MAIC from tuberculous mycobacteria (11, 20). An anti-GPL antibody is produced in the sera of patients and reflects the disease, which is useful in diagnosis and treatment (21, 22, 25). Moreover, it was reported that ethambutol-susceptible and -resistant MAIC strains of serotype 1 had different GPL profiles. The susceptible strain expressed only the polar serotype 1 GPL, and the resistant strain expressed several apolar GPLs. The efficacy of antibiotics may be affected by the GPL profile through differences in cell wall permeability (19). On the other hand, the importance of TLR-mediated responses has been studied in tuberculous infections. Means et al. (28) reported that *M. tuberculosis* activated both TLR2 and TLR4, whereas heat-killed *M. tuberculosis* and *M. avium* activated only TLR2. It was observed that MyD88- and TLR2-deficient mice have increased susceptibility to *M. avium* infection compared to TLR4-deficient and wild-type mice (12). These lines of evidence suggest that TLRs are related to host recognition of the MAIC components containing GPLs and affect MAIC infections. Brennan and Goren (6) first proposed that GPLs were alkaline-stable lipids and made it possible to classify serospecificity by the unique, variable deacetylated OSE sequences (9). We did not detect any biological activity of these alkaline-treated GPLs on splenocytes and bone marrow macrophages of mice in *in vitro* stimulation. Recently, Schorey and colleagues (35, 36) clarified that serotype 1 and 2 GPLs can function as TLR2 agonists and promote macrophage activation in a TLR2- and MyD88-dependent pathway. They reported that the acetylated and methylated groups of GPLs were necessary for GPL-TLR2 interaction as a molecular requirement. In this study, we purified both native and alkaline-treated serotype 13 GPLs and clarified the acetylation patterns of serotype 13 GPL. It was confirmed that the native acetylated form of serotype 13 GPL was recognized via TLR2 and that the deacetylated form by alkaline treatment was not recognized. The serotype 13 GPL has one *O*-methyl group next to the terminal *N*-acylated Hex that was stable regardless of alkaline treatment. Taken together, an acetyl rather than a methyl group was necessary for host immune response via TLR2. The completely acetylated derivative of alkaline-treated serotype 13 GPL partially recovered the HEK-blue-2 activation, compared to the native form containing 2 to 4 acetylated groups. It may be important for GPL-TLR2 interaction to balance the hydrophobicity and hydrophilicity of the molecule. Recht and Kolter (32) reported that the acetylation of GPL affects sliding motility and biofilm formation by deleting the *atf1* gene, which is responsible for acetylation on the 6-d-Tal of GPL core in *Mycobacterium smegmatis*. Rhoades et al. (33) reported that the *Mycobacterium abscessus* GPLs were related to smooth and rough colony morphology and that the GPLs in the outermost portion of the cell wall masked underlying phosphatidyl-*myo*-inositol mannosides involved in stimulating the innate immune response via TLR2. In contrast, our results suggest that the species-specific acetylated GPL is effective in host recognition as a TLR2 agonist independent of phosphatidyl-*myo*-inositol mannosides and that it plays important roles directly in host innate immune responses. Regulating the acetylation of GPL may control the MAIC pathogenicity by, for example, developing the inhibitor of ATF1.

The present study demonstrated the chemical structure and biosynthesis gene cluster of the serotype 13 GPL of *M. intracellulare* and host innate immune response via TLR2. Serotype 13 GPL should be included in group 2 GPLs, and the phylogenetic relationship of serotype 7, 12, and 13 strains was par-

tially clarified by the GPL. We propose that the lipid components in the cell envelope are important for MAIC infection and that the structure modification must be taken into account. These findings shed light on the better understanding of the structure-function relationships of GPLs and may open a new avenue for the prevention of MAIC infections.

ACKNOWLEDGMENTS

This work was supported by grants from the Ministry of Education, Culture, Sports, Science and Technology of Japan, the Japan Health Sciences Foundation, and the Ministry of Health, Labor and Welfare of Japan (Research on Emerging and Reemerging Infectious Diseases).

REFERENCES

1. **Aspinall, G. O., D. Chatterjee, and P. J. Brennan.** 1995. The variable surface glycolipids of mycobacteria: structures, synthesis of epitopes, and biological properties. Adv. Carbohydr. Chem. Biochem. **51:**169–242.
2. **Belisle, J. T., K. Klaczkiewicz, P. J. Brennan, W. R. Jacobs, Jr., and J. M. Inamine.** 1993. Rough morphological variants of *Mycobacterium avium*. Characterization of genomic deletions resulting in the loss of glycopeptidolipid expression. J. Biol. Chem. **268:**10517–10523.
3. **Bhatnagar, S., and J. S. Schorey.** 2007. Exosomes released from infected macrophages contain *Mycobacterium avium* glycopeptidolipids and are proinflammatory. J. Biol. Chem. **282:**25779–25789.
4. **Bhatt, A., et al.** 2007. Deletion of kasB in *Mycobacterium tuberculosis* causes loss of acid-fastness and subclinical latent tuberculosis in immunocompetent mice. Proc. Natl. Acad. Sci. U. S. A. **104:**5157–5162.
5. **Bozic, C. M., M. McNeil, D. Chatterjee, L Jardine, and P. J. Brennan.** 1988. Further novel amido sugars within the glycopeptidolipid antigens of *Mycobacterium avium*. J. Biol. Chem. **263:**14984–14991.
6. **Brennan, P. J., and M. B. Goren.** 1979. Structural studies on the type-specific antigens and lipids of the *Mycobacterium avium-Mycobacterium intracellulare-Mycobacterium scrofulaceum* serocomplex. *Mycobacterium intracellulare* serotype 9. J. Biol. Chem. **254:**4205–4211.
7. **Brennan, P. J., M. Heifets, and B. P. Ullom.** 1982. Thin-layer chromatography of lipid antigens as a means of identifying nontuberculous mycobacteria. J. Clin. Microbiol. **15:**447–455.
8. **Brennan, P. J., and H. Nikaido.** 1995. The envelope of mycobacteria. Annu. Rev. Biochem. **64:**29–63.
9. **Chatterjee, D., and K. H. Khoo.** 2001. The surface glycopeptidolipids of mycobacteria: structures and biological properties. Cell. Mol. Life Sci. **58:** 2018–2042.
10. **Eckstein, T. M., J. T. Belisle, and J. M. Inamine.** 2003. Proposed pathway for the biosynthesis of serovar-specific glycopeptidolipids in *Mycobacterium avium* serovar 2. Microbiology **149:**2797–2807.
11. **Enomoto, K., et al.** 1998. Rapid serodiagnosis of *Mycobacterium avium-intracellulare* complex infection by ELISA with cord factor (trehalose 6, 6′-dimycolate), and serotyping using the glycopeptidolipid antigen. Microbiol. Immunol. **42:**689–696.
12. **Feng, C. G., et al.** 2003. Mice lacking myeloid differentiation factor 88 display profound defects in host resistance and immune responses to *Mycobacterium avium* infection not exhibited by Toll-like receptor 2 (TLR2)- and TLR4-deficient animals. J. Immunol. **171:**4758–4764.
13. **Fujiwara, N., et al.** 2007. Structural characterization of a specific glycopeptidolipid containing a novel *N*-acyl-deoxy sugar from *Mycobacterium intracellulare* serotype 7 and genetic analysis of its glycosylation pathway. J. Bacteriol. **189:**1099–1108.
14. **Fujiwara, N., et al.** 2008. Structural analysis and biosynthesis gene cluster of an antigenic glycopeptidolipid from *Mycobacterium intracellulare*. J. Bacteriol. **190:**3613–3621.
15. **Hakomori, S.** 1964. A rapid permethylation of glycolipid, and polysaccharide catalyzed by methylsulfinyl carbanion in dimethyl sulfoxide. J. Biochem. **55:**205–208.
16. **Howard, S. T., et al.** 2006. Spontaneous reversion of *Mycobacterium abscessus* from a smooth to a rough morphotype is associated with reduced expression of glycopeptidolipid and reacquisition of an invasive phenotype. Microbiology **152:**1581–1590.
17. **Kaufmann, S. H.** 2001. How can immunology contribute to the control of tuberculosis? Nat. Rev. Immunol. **1:**20–30.
18. **Khoo, K. H., et al.** 1996. Novel *O*-methylated terminal glucuronic acid characterizes the polar glycopeptidolipids of *Mycobacterium habana* strain TMC 5135. J. Biol. Chem. **271:**12333–12342.
19. **Khoo, K. H., et al.** 1999. Altered expression profile of the surface glycopeptidolipids in drug-resistant clinical isolates of *Mycobacterium avium* complex. J. Biol. Chem. **274:**9778–9785.
20. **Kitada, S., et al.** 2008. Serodiagnosis of *Mycobacterium avium*-complex pulmonary disease using an enzyme immunoassay kit. Am. J. Respir. Crit. Care Med. **177:**793–797.
21. **Kitada, S., et al.** 2010. Serodiagnosis of pulmonary disease due to *Mycobacterium avium* complex proven by bronchial wash culture. Chest **138:**236–237.
22. **Kitada, S., et al.** 2007. Serological test and chest computed tomography findings in patients with *Mycobacterium avium* complex lung disease. Eur. Respir. J. **29:**1217–1223.
23. **Krzywinska, E., J. Krzywinski, and J. S. Schorey.** 2004. Phylogeny of *Mycobacterium avium* strains inferred from glycopeptidolipid biosynthesis pathway genes. Microbiology **150:**1699–1706.
24. **Krzywinska, E., and J. S. Schorey.** 2003. Characterization of genetic differences between *Mycobacterium avium* subsp. *avium* strains of diverse virulence with a focus on the glycopeptidolipid biosynthesis cluster. Vet. Microbiol. **91:**249–264.
25. **Maekura, R., et al.** 2005. Clinical and prognostic importance of serotyping *Mycobacterium avium-Mycobacterium intracellulare* complex isolates in human immunodeficiency virus-negative patients. J. Clin. Microbiol. **43:**3150–3158.
26. **Marras, T. K., and C. L. Daley.** 2002. Epidemiology of human pulmonary infection with nontuberculous mycobacteria. Clin. Chest Med. **23:**553–567.
27. **Matsunaga, I., T. Komori, A. Ochi, N. Mori, and M. Sugita.** 2008. Identification of antibody responses to the serotype-nonspecific molecular species of glycopeptidolipids in *Mycobacterium avium* infection. Biochem. Biophys. Res. Commun. **377:**165–169.
28. **Means, T. K., et al.** 1999. Human Toll-like receptors mediate cellular activation by *Mycobacterium tuberculosis*. J. Immunol. **163:**3920–3927.
29. **Miyamoto, Y., et al.** 2010. Novel rhamnosyltransferase involved in biosynthesis of serovar 4-specific glycopeptidolipid from *Mycobacterium avium* complex. J. Bacteriol. **192:**5700–5708.
30. **Nakata, N., et al.** 2008. Identification and characterization of two novel methyltransferase genes that determine the serotype 12-specific structure of glycopeptidolipids of *Mycobacterium intracellulare*. J. Bacteriol. **190:**1064–1071.
31. **Primm, T. P., C. A. Lucero, and J. O. Falkinham III.** 2004. Health impacts of environmental mycobacteria. Clin. Microbiol. Rev. **17:**98–106.
32. **Recht, J., and R. Kolter.** 2001. Glycopeptidolipid acetylation affects sliding motility and biofilm formation in *Mycobacterium smegmatis*. J. Bacteriol. **183:**5718–5724.
33. **Rhoades, E. R., et al.** 2009. *Mycobacterium abscessus* glycopeptidolipids mask underlying cell wall phosphatidyl-myo-inositol mannosides blocking induction of human macrophage TNF-alpha by preventing interaction with TLR2. J. Immunol. **183:**1997–2007.
34. **Schorey, J. S., and L. Sweet.** 2008. The mycobacterial glycopeptidolipids: structure, function, and their role in pathogenesis. Glycobiology **18:**832–841.
35. **Sweet, L., and J. S. Schorey.** 2006. Glycopeptidolipids from *Mycobacterium avium* promote macrophage activation in a TLR2- and MyD88-dependent manner. J. Leukoc. Biol. **80:**415–423.
36. **Sweet, L., et al.** 2008. *Mycobacterium avium* glycopeptidolipids require specific acetylation and methylation patterns for signaling through Toll-like receptor 2. J. Biol. Chem. **283:**33221–33231.
37. **Tsang, A. Y., J. C. Denner, P. J. Brennan, and J. K. McClatchy.** 1992. Clinical and epidemiological importance of typing of *Mycobacterium avium* complex isolates. J. Clin. Microbiol. **30:**479–484.
38. **Tsang, A. Y., I. Drupa, M. Goldberg, J. K. McClatchy, and P. J. Brennan.** 1983. Use of serology and thin-layer chromatography for the assembly of an authenticated collection of serovars within the *Mycobacterium avium-Mycobacterium intracellulare-Mycobacterium scrofulaceum* complex. Int. J. Syst. Bacteriol. **33:**285–292.
39. **Wagner, D., and L. S. Young.** 2004. Nontuberculous mycobacterial infections: a clinical review. Infection **32:**257–270.

ANTIMICROBIAL AGENTS AND CHEMOTHERAPY, Sept. 2011, p. 4000–4005 Vol. 55, No. 9
0066-4804/11/$12.00 doi:10.1128/AAC.00434-11

Apoptosis-Inducing Activity of Clofazimine in Macrophages[▽]

Yasuo Fukutomi,* Yumi Maeda, and Masahiko Makino

Leprosy Research Center, National Institute of Infectious Diseases, 4-2-1, Aoba-cho, Higashimurayama-shi, Tokyo 189-0002, Japan

Received 1 April 2011/Returned for modification 19 May 2011/Accepted 9 June 2011

Clofazimine is a riminophenazine compound which has been used for the treatment of leprosy since the 1960s. Although the drug is effective in the management of leprosy reactions because of its anti-inflammatory activity, the mechanism leading to the cessation of inflammation is not well understood. In the present study, it was shown that clofazimine exhibits apoptosis-inducing activity in macrophages. When human monocyte-derived macrophages were cultured *in vitro* in the presence of clofazimine, the cells exhibited a marked decrease in metabolic activity and showed shrinkage in cell size, indicating cell death. Nuclear condensation and fragmentation were also observed by Giemsa and Hoechst 33248 stains. The endonuclease inhibitor $ZnCl_2$ inhibited the clofazimine-induced cell death. Significant enhancement of caspase-3 activity was observed in clofazimine-treated macrophages and THP-1 cells. Collectively, these results suggest the apoptosis-inducing activity of clofazimine in macrophages, which may also be responsible for the antibacterial properties of clofazimine.

Clofazimine (B663) is a phenazine iminoquinone derivative, specifically, a riminophenazine dye with the empirical formula $C_{27}H_{22}C_{12}$. In the 1950s, Barry et al. synthesized a large number of compounds by progressive chemical alteration of the anilinoaposafranine molecule, several of which showed antituberculous activity both *in vitro* and in experimental animals (1). Of these compounds, clofazimine (or Lamprene or B663) was found to be highly active against mycobacteria with the least toxicity. Chang (4) observed the antibacterial activity of clofazimine against *Mycobacterium lepraemurium* at about the same time as its anti-*M. leprae* activity was reported by Browne (2) and Browne and Hogenzeil (3). Later, after the introduction of the mouse footpad method of Shepard and Chang (22), its antibacterial activity against *M. leprae* was demonstrated (18).

Clofazimine has bifunctional activity: antibacterial and anti-inflammatory. It was used in the treatment of leprosy for its antibacterial action against *M. leprae*. Later, it was also found to possess an anti-inflammatory action which makes it a very useful drug in the treatment of acute reactions, including erythema nodosum leprosum (ENL), neuritis, iritis, etc., although its mechanism of action is unknown (2). *In vitro* studies on the effect of clofazimine on immune cells have been conducted. Clofazimine increases superoxide anion production and degranulation by stimulated neutrophils. and tumor necrosis factor alpha (TNF-α) potentiates this enhancement (15). The mechanism underlying this pro-oxidative effect seems to involve stimulation of phospholipase A2 (PLA2) activity with subsequent accumulation of arachidonic acid and lysophospholipids, which act as second messengers to activate oxidase (10). In addition, a number of reports have demonstrated the effects of clofazimine that might predict increased immune activity. Lysosomal enzyme activity of cultured macrophages was upregulated by clofazimine (21). Peripheral blood monocytes from healthy volunteers have been demonstrated to exhibit increased major histocompatibility complex class II expression following incubation with clofazimine (25). Increased oxygen uptake during phagocytosis was observed in neutrophils derived from patients with pyoderma gangrenosum during clofazimine therapy (5). Suppressor T-cell activity was decreased in mycobacteria-infected mice during clofazimine treatment (26). However, the mechanisms underlying the anti-inflammatory action of clofazimine are still unclear.

In the present study, we examined the effect of clofazimine on macrophages and found that the drug possessed apoptosis-inducing activity.

MATERIALS AND METHODS

Drug and chemicals. Clofazimine (Sigma-Aldrich Co., St. Louis, MO), rifampin (catalog no. R3501; Sigma-Aldrich Co.), and dapsone (DDS; Biomol Research Inc., Butler Pike Plymouth Meeting, PA) were dissolved in dimethyl sulfoxide (DMSO) and stored at −30°C until use. Ampicillin was obtained from Sigma-Aldrich Co.

Culture of human macrophages and isolation of bacilli. Human peripheral blood was obtained under informed consent from healthy individuals. Peripheral blood mononuclear cells (PBMCs) were isolated using Ficoll-Paque Plus (GE Healthcare Life Sciences, Buckinghamshire, United Kingdom) gradient centrifugation (12). The cells were suspended in AIM-V medium (Gibco BRL, Invitrogen Corp., Carlsbad, CA), and 1×10^6 PBMCs were cultured in a well of a 24-well tissue culture plate (Falcon; Becton Dickinson Labware, Becton Dickinson and Company, Franklin Lakes, NJ) containing 13-mm round coverslips (Nunc Thermanox coverslips; Nalge Nunc, Thermo Scientific, Rochester, NY) at 37°C in a 5% CO_2 incubator for adherence of monocytes. After 1 h incubation, the coverslips were washed with Hanks' balanced salt solution (HBSS; Sigma-Aldrich Co.) to remove nonadherent cells. The monocytes on the coverslips were cultured in a new 24-well plate containing RPMI 1640 medium (Sigma-Aldrich Co.) supplemented with 25 mM HEPES, 10% fetal bovine serum (FBS; Bio Whittaker Co., Walkersville, MD), 2 mM L-glutamine, and 100 μg/ml ampicillin (RPMI-10F) in the presence of 40 ng/ml of granulocyte-macrophage colony-stimulating factor (R&D Systems, Minneapolis, MN). After 10 days, the cells were differentiated into macrophages and used for experiments. In some experiments, PBMCs were cultured in 35-mm cell culture dishes (Corning Inc., Corning, NY) for adherence, and adherent monocytes were cultured for 10 days. Human monocytic leukemia cell line THP-1 was maintained in RPMI 1640 medium containing 15% fetal bovine serum.

* Corresponding author. Mailing address: Leprosy Research Center, National Institute of Infectious Diseases, 4-2-1, Aoba-cho, Higashimurayama-shi, Tokyo 189-0002, Japan. Phone: 81-42-391-8211. Fax: 81-42-394-9092. E-mail: fukutomi@nih.go.jp.

▽ Published ahead of print on 20 June 2011.

M. leprae (Thai-53 strain) was isolated from the footpads of BALB/c *nu/nu* mice that had been inoculated with *M. leprae* 8 months prior to isolation, and the bacillary number was enumerated according to the method of Shepard and Chang (22).

Light and phase-contrast microscopy. Macrophages on the coverslip were fixed with absolute methanol, followed by performing Giemsa stain (Wako Co., Japan). After they were mounted on a glass slide, the cells were observed under a light microscope (Optiphot-2; Nikon Co., Tokyo, Japan). Photographs were taken with a digital camera (Nikon F70s). Macrophages in 35-mm dishes were incubated in the presence of clofazimine and observed under a phase-contrast microscope (Olympus CKX41 with ×10- and ×20-objective lenses). Photographs were taken with an Olympus DP50 system. Image acquisition and data processing were done using the DP controller software.

Fluorescence microscopy. Fluorescence staining for DNA was employed. Macrophages were cultured in an 8-well chamber slide (Lab-Tek II chamber slide system; Nalge Nunc). The cells were incubated in the presence of clofazimine and subsequently fixed with 2.5% glutaraldehyde in phosphate-buffered saline (PBS). Hoechst 33342 dye (Sigma-Aldrich Co.) in PBS was added to the wells at a final concentration of 10 μM, and the slide was incubated for 1 h at 37°C. The cells on the slide were observed under a fluorescence microscope (Olympus BX60 with a ×40-objective lens) equipped with an Olympus DP50 system. The digital images were processed with DP controller software.

Determination of cell death. Cell viability was determined using the colorimetric method (Cell Titer 96 aqueous nonradioactive cell proliferation assay; Promega Corp., Madison, WI). Briefly, cells in a 24-well plate were incubated in the presence of clofazimine in phenol red-free RPMI 1640 medium containing 10% FBS, followed by addition of 3-(4,5-dimethylthiazol-2-yl)-5-(3-carboxymethoxyphenyl)-2-(4-sulfophenyl)-2*H*-tetrazolium, inner salt/phenazine methosulfate solution (formazan reagent). After 1 h incubation at 37°C, an aliquot of medium was transferred into a well of a 96-well plate, and the developed color was measured by a microplate reader at 490 nm. In addition, the activity of lactate dehydrogenase (LDH), released from dead cells into culture supernatants, was measured by a colorimetric assay (Cytotox 96 nonradioactive cytotoxicity assay; Promega Corp.). The color that developed in a sample incubated with LDH substrate was measured by a microplate reader at 490 nm (Vmax; Molecular Devices Corp., Sunnyvale, CA).

DNA electrophoresis. THP-1 cells or macrophages were harvested from the culture, and DNA was purified by a spin column method (E.Z.N.A. tissue DNA kits; Omega Bio-Tek, Norcross, GA). Briefly, 5×10^6 cells incubated in the presence of clofazimine were harvested, centrifuged at 2,000 rpm for 5 min, washed once with PBS, and resuspended in PBS. Protease was added, the mixture was heated at 65°C for 5 min, and buffer BL was added. After the mixture was heated at 70°C for 10 min, ethanol was further added. The mixture was applied to a HiBind spin column and centrifuged. DNA bound to the column was finally eluted, and the DNA preparation was subjected to electrophoresis in a 1% agarose gel, followed by ethidium bromide staining, and DNA was visualized by UV transillumination.

Western blotting. THP-1 cells or macrophages incubated with clofazimine were washed once with PBS(−) and lysed in lysis buffer (CelLytic-M; Sigma-Aldrich Co.) containing 2 protease inhibitor cocktails (phosphatase inhibitor cocktail 1 and phosphatase inhibitor cocktail 2; Sigma-Aldrich Co.). In the case of clofazimine-treated adherent macrophages, the cells were scraped off the dishes with a rubber policeman. The lysates were incubated for 10 min on ice and centrifuged at 13,000 rpm for 5 min. The protein concentration was determined. Ten micrograms of total protein was loaded onto an SDS-PAGE gel. After running the electrophoresis, the proteins in the gel were transferred onto an Immobilon PSQ membrane (Millipore Corporation, Billerica, MA). After washing with Tris-buffered saline (2.42 g Tris base and 8 g NaCl per 1 liter, pH 7.6) containing 0.05% Tween 20 (TBS-T), the membrane was blocked with 5% skim milk (Amersham ECL Plus Western blotting reagent pack; GE Healthcare Life Sciences, Amersham Place, Buckinghamshire, United Kingdom) for 1 h at room temperature. The membrane was washed 3 times with TBS-T and incubated overnight with 1:3,000-diluted primary anticleaved caspase-3 antibody (cleaved caspase antibody sampler kit; Cell Signaling Technology Inc., Danvers, MA). The membrane was then incubated with 1:10,000-diluted horseradish peroxidase (HRP)-conjugated secondary antibody for 1 h at room temperature. Finally, proteins were detected by incubating the membrane with HRP substrate (Immobilon Western chemiluminescent HRP substrate; Millipore Corporation), and the membrane was exposed to X-ray film (Amersham Hyperfilm ECL; GE Healthcare). For reprobing of the membrane, the membrane was washed with TBS-T and incubated with stripping buffer (Restore Plus Western blot stripping buffer; Pierce, IL). After the membrane was blocked, it was used again for probing different antibodies, such as cleaved caspase-9 and poly(ADP-ribose) polymerase (PARP) antibodies (cleaved caspase antibody sampler kit; Cell Signaling Technology Inc.) and beta-actin antibody (Cell Signaling Technology Inc.).

Colorimetric caspase assay. Colorimetric substrates for caspases were used to determine caspase-3 activity (colorimetric caspase assay kits; Biovision Research Products, CA) in lysates of cells incubated in the presence of clofazimine. Briefly, 5×10^6 cells were pelleted and lysed with chilled lysis buffer. After centrifugation, the supernatant was transferred to a new tube, and reaction buffer and a substrate for caspase-3, Asp-Glu-Val-Asp–*p*-nitroanilide, were added to the tube. After incubation for 2 h at 37°C, the samples were transferred into a well of a 384-well plate and read by a plate reader at 405 nm (Infinite F200; Tecan Systems Inc., San Jose, CA). The background reading was obtained by subtracting the reading for the reaction buffer from the reading for the lysate samples.

PGE_2 assay. The amount of prostaglandin E_2 (PGE_2) in the culture supernatants was measured by enzyme-linked immunosorbent assay (catalog no. 514010; Cayman Chemical Co., MI).

RESULTS

Morphological changes observed after treatment with clofazimine. Macrophages differentiated from human monocytes were incubated in the presence of 10 μg/ml of clofazimine for 20 h. The change in cell morphology was observed under a phase-contrast microscope. As shown in Fig. 1B, in the presence of clofazimine, the cells exhibited shrinkage in cell size and membrane blebbing. The death of more than 80% of cells was observed (Fig. 1B). As a control, Fig. 1A shows the normal morphology of macrophages. By Giemsa stain, too, these clofazimine-treated cells exhibited shrinkage in cell size, accompanied by the appearance of fragmented smaller nuclei (arrow in Fig. 1D), suggesting the apoptotic nature of the cells. Nontreated macrophages showed intact nuclei (arrow in Fig. 1C). Again, the change of nuclear structure was confirmed by Hoechst dye staining. Under a fluorescence microscope, nuclear condensation and membrane blebbing were observed in the clofazimine-treated cells (Fig. 1F and G), in contrast to normal cells, which showed intact nuclei (Fig. 1E). Similar fragmentation or condensation of chromatin was observed in THP-1 cells (data not shown). Such morphological changes were not observed in THP-1 cells treated with rifampin or dapsone at a concentration up to 50 μg/ml. Also, DMSO, which was used as a solvent for clofazimine at a concentration of 0.2%, had no effect on cell morphology or cell functions (negative control).

Cell death-inducing activity of clofazimine determined by colorimetric assay. Cell death was determined by a biochemical analysis using a colorimetric method. The conversion of the tetrazolium compound into soluble formazan is accomplished by metabolically active cells. When higher concentrations up to 10 μg/ml of clofazimine were employed in macrophage cultures, decreased color intensity of soluble formazan was observed, indicating cell death (Fig. 2A). Cell death was also observed in THP-1 cells (Fig. 2B). Hansen's disease is caused by infection of macrophages with *M. leprae*; therefore, we are curious to know whether *M. leprae* infection affects the cell death-inducing activity of clofazimine. When we infected macrophages with *M. leprae* at a multiplicity of infection (MOI) of 10 or 30, we found no significant difference in the induction of cell death in the presence of 10 μg/ml clofazimine, indicating that the bacilli did not inhibit or enhance clofazimine-induced cell death (Fig. 2C). Another method of determining cell death is by measurement of LDH release from

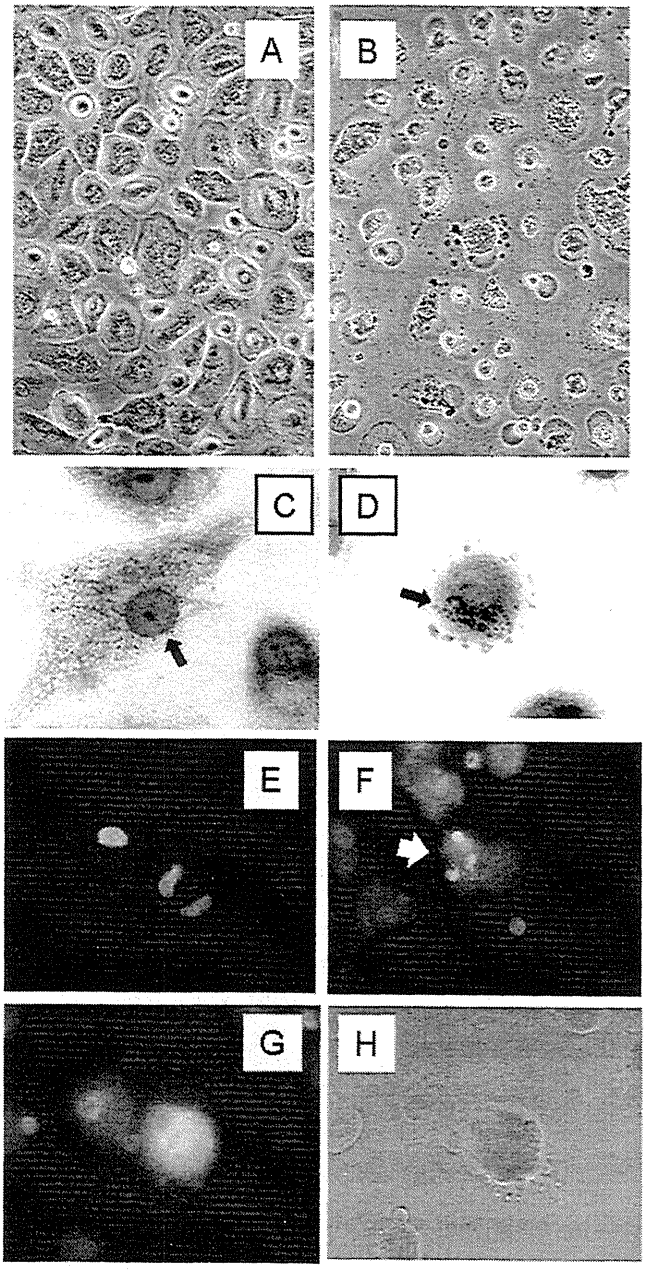

FIG. 1. Cell death induced in macrophages by clofazimine. Photographs were taken under a phase-contrast microscope (A and B) with a ×20-objective lens. (B) Human monocyte-derived macrophages were incubated in the presence of 10 μg/ml of clofazimine for 20 h. (A) Cells cultured in the absence of clofazimine showed normal morphology. Giemsa stain of clofazimine-treated macrophages was also performed (C and D). Human monocyte-derived macrophages were incubated in the presence of 10 μg/ml of clofazimine (D) or in the absence of clofazimine (C) for 24 h. Photographs were taken under a light microscope with a ×100-objective lens. Fragmentation of the nucleus was significant in the clofazimine-treated cells (arrow in panel D), in contrast to the intact morphology of the nucleus in normal cells (arrow in panel C). Nuclear condensation and fragmentation of clofazimine-treated macrophages were also confirmed under a fluorescence microscope (E to G). Macrophages were incubated in the presence of 10 μg/ml of clofazimine, followed by fixation and stained with a nucleus-staining dye, Hoechst 33342. The cells were observed under a fluorescence microscope (×40-objective lens). Cells cultured without clofazimine (E), clofazimine-treated cells (F and G), and a phase-contrast image of panel G (H) are shown.

dead cells. As shown in Fig. 3, more LDH release was observed in the manner dependent on the concentration of clofazimine.

Clofazimine treatment induces DNA ladder formation in macrophages. We examined the condition of DNA in clofazimine-treated THP-1 cells. Agarose gel electrophoresis showed fragmentation of DNA into integer multiples of 180 bp, a so-called DNA ladder (Fig. 4A), suggesting that DNA endonuclease was activated by clofazimine treatment. Therefore, we examined the effect of one of the apoptosis inhibitors, $ZnCl_2$, which is known to possess suppressing activity for endonuclease, and found that clofazimine-induced DNA fragmentation in THP-1 cells was completely blocked by $ZnCl_2$ treatment even at a low concentration of 0.25 mM $ZnCl_2$ (Fig. 4B), although it is still not clear whether $ZnCl_2$ can directly block the activity of clofazimine. Moreover, it was evident that neither cell death nor DNA fragmentation was induced by other antileprosy drugs, such as DDS or rifampin (Fig. 4C).

Clofazimine-induced cell death is mediated by activation of caspase-3. Caspases are known to be central regulators of apoptotic cell death, and caspase-3, which locates downstream of the caspase pathway, is one of the key executioners of apoptosis. Upon apoptotic stimulation, caspases are cleaved into active fragments. Figure 5 shows a Western blot analysis of extracts from THP-1 cells and macrophages cultured in the presence of clofazimine. Enhanced expression of cleaved caspase-3 was detected in cells (Fig. 5A and B). In addition, caspase-9 was also cleaved. A DNA-repairing enzyme, PARP, which is cleaved by caspase-3, was significantly activated in clofazimine-treated THP-1 cells (Fig. 5A). We next measured the caspase activity by colorimetric assay (Fig. 5C). The induction of caspase-3 by clofazimine was significantly high in macrophages as well as THP-1 cells.

Clofazimine enhanced PGE_2 production in *M. leprae*-infected macrophages. Monocyte-derived macrophages were preincubated in the presence of clofazimine for 4 h, followed by replenishment with *M. leprae*-containing medium for 20 h. The culture supernatants were collected, and the PGE_2 concentration was measured. As shown in Fig. 6, clofazimine clearly enhanced PGE_2 production in macrophages.

DISCUSSION

Riminophenazines are structurally phenazine compounds which were derived from lichens historically and were targeted for treatment of tuberculosis. The first clinically developed phenazine compound was clofazimine, whose activity has been extended to other mycobacterial diseases (1, 17). In test animals, the drug was found to inhibit the growth of mycobacteria *in vivo*, as well as *in vitro* (22), but the molecular mechanism of clofazimine in inducing anti-*M. leprae* activity is still not yet clear.

In the present study, it was found that both human monocyte-derived macrophages and THP-1 cells exhibited marked decreases in their metabolic activity in the presence of 10 μg/ml clofazimine. Under a phase-contrast microscope, 80% of the cells showed irregular morphology with shrinkage in cell size, and by a precise time course study, it was revealed that the morphological changes were evident from 6 h incubation with clofazimine. From this early time point, the cell body began to shrink, accompanied by membrane blebbing, which was also

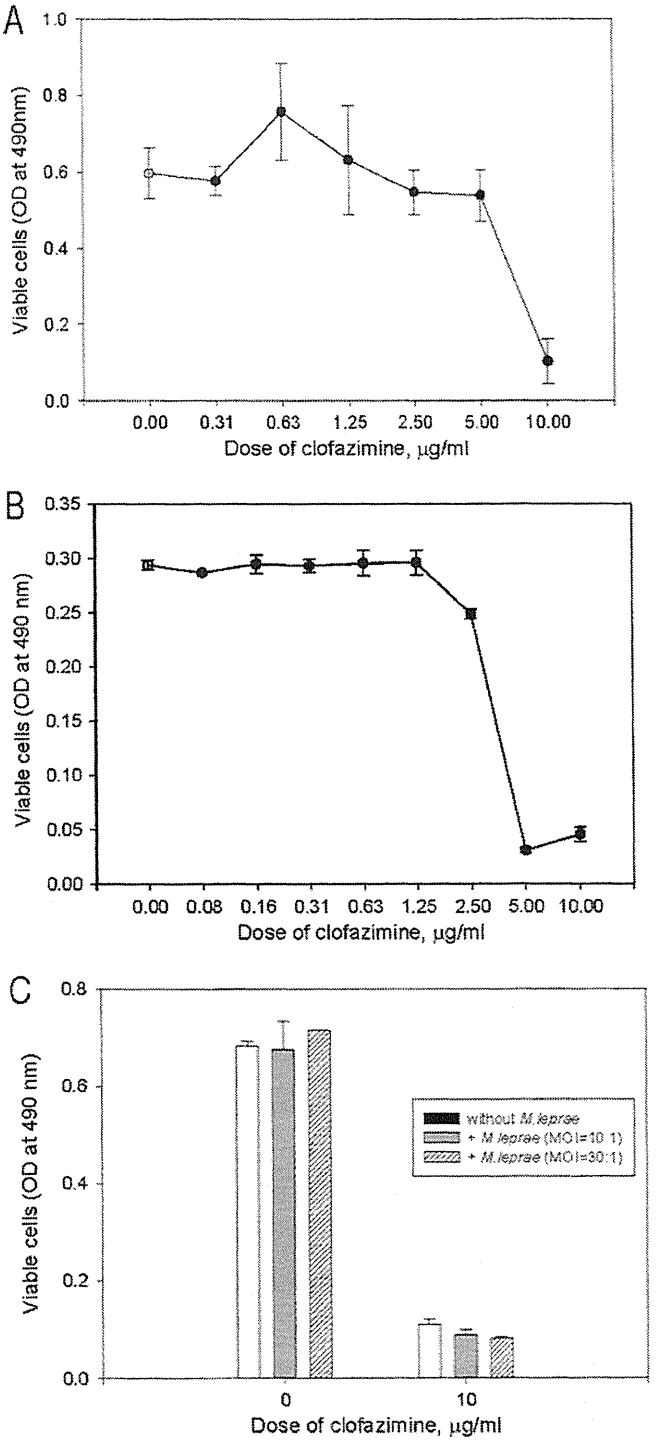

FIG. 2. Clofazimine-induced cell death in macrophages and THP-1 cells. Human monocyte-derived macrophages (A) and THP-1 cells (B) were incubated with various concentrations of clofazimine for 24 h, followed by determination of viable cells by the Cell Titer 96 cell proliferation assay. The results are representative of three independent cell culture tests. The cell death-inducing effect of clofazimine in the presence of *M. leprae* was also examined. Monocyte-derived macrophages were infected with *M. leprae* at an MOI of 10 or 30 per cell for 24 h. The infected cells were further incubated with 10 μg/ml clofazimine for another 24 h, followed by determination of viable cells by Cell Titer 96 cell proliferation assay (C). The results are representative of three independent cell culture tests. OD, optical density.

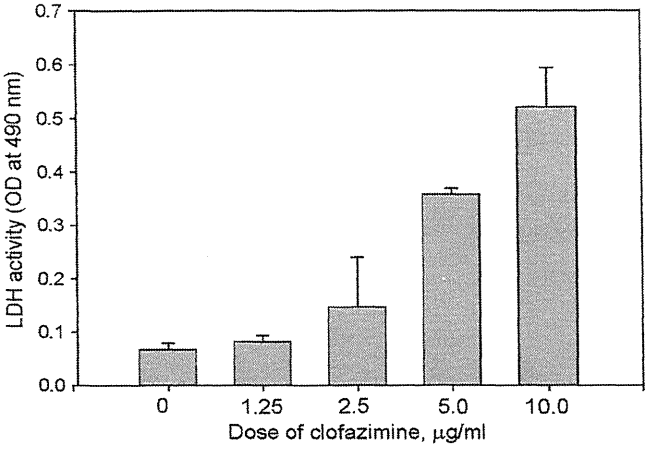

FIG. 3. LDH release from clofazimine-treated macrophages. Human monocyte-derived macrophages were incubated in the presence of the indicated concentrations of clofazimine for 24 h, and the LDH activity was measured. The results were obtained from triplicate cultures and are representative of three independent cell culture tests. OD, optical density.

evident from Giemsa stain and Hoechst staining of the nuclei (Fig. 1). Interestingly, the dose of clofazimine (10 μg/ml) required to cause cell death was equivalent to the dose required to exhibit anti-*M. leprae* activity *in vitro* by radiorespirometry (data not shown), the dose of which is in concordance with the dose required to kill *M. leprae* reported by Franzblau and O'Sullivan (7). Moreover, in our study, at 5-μg/ml concentrations of clofazimine, *M. leprae* viability was lowered in *in vitro* experiments with *M. leprae*-infected macrophages, and with this dose, *M. leprae* was found not to inhibit clofazimine-induced cell death. Therefore, clofazimine might inhibit mycobacterial growth through an alternative way by inducing apoptosis of host cells. Although the concentration of clofazimine in sera of patients taking regular doses of the drug is as low as 1 to 2 μg/ml, fat-soluble clofazimine readily accumulates in cells. In one patient, 7 months treatment with clofazimine (200 mg/day) resulted in accumulation of needle-shaped crystal inclusions in his alveolar macrophages (20). In another report, clofazimine-induced crystal-storing histiocytosis was observed in a leprosy patient (23). So, we are of the opinion that in some cells, the concentration of clofazimine is higher (10 to 20 μg/ml) than in others, so we have used a concentration of 10 μg/ml for our experiments.

Normally, cells undergo distinct morphological changes when they progress through either necrosis or apoptosis. Necrosis occurs when cells are exposed to an extreme variance from physiological conditions, resulting in damage to the plasma membrane. As such, necrosis is characterized by cell swelling and disruption of cellular organelles, with little change in the chromatin initially. In contrast, apoptotic cells shrink in size, undergo membrane blebbing, and exhibit marked alterations in their chromatin structure at an early stage under normal physiological conditions. As mentioned earlier, treatment with clofazimine resulted in highly condensed chromatin within the nucleus and membrane blebbing, indicating macrophages undergoing apoptosis. To confirm this, DNA from clofazimine-treated THP-1 cells was examined. Fragmented DNA was

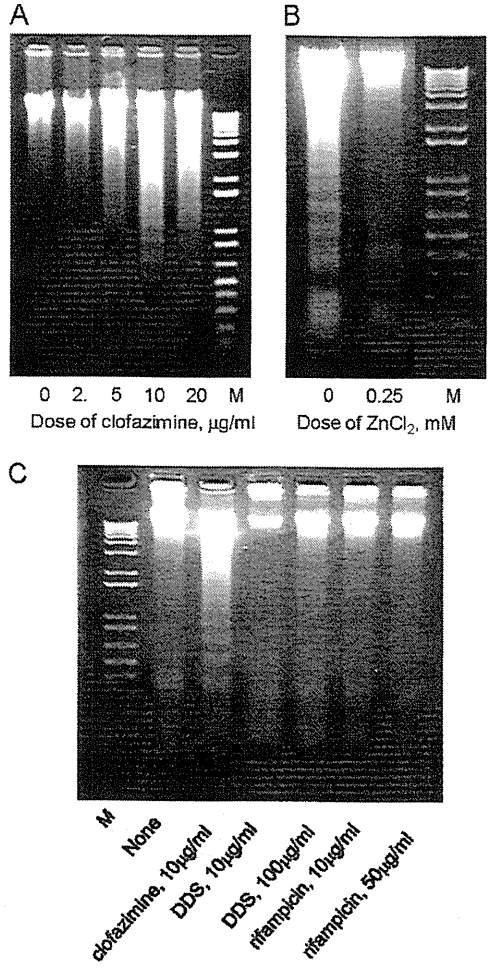

FIG. 4. DNA ladder formation in clofazimine-treated THP-1 cells and effects of other antileprosy drugs on DNA ladder formation. (A) THP-1 cells were incubated in the presence of the indicated concentrations of clofazimine for 4 h, followed by purification of DNA for agarose gel electrophoresis. An ethidium bromide-stained agarose gel is shown. (B) An endonuclease inhibitor, $ZnCl_2$, was examined for its effect on clofazimine-induced ladder formation. THP-1 cells were incubated in the presence of 10 μg/ml clofazimine and $ZnCl_2$ for 4 h. DNA was purified for electrophoresis. (C) THP-1 cells were incubated in the presence of clofazimine, DDS, and rifampin for 4 h, followed by purification of DNA. An ethidium bromide-stained agarose gel is shown. Lanes M, molecular weight marker.

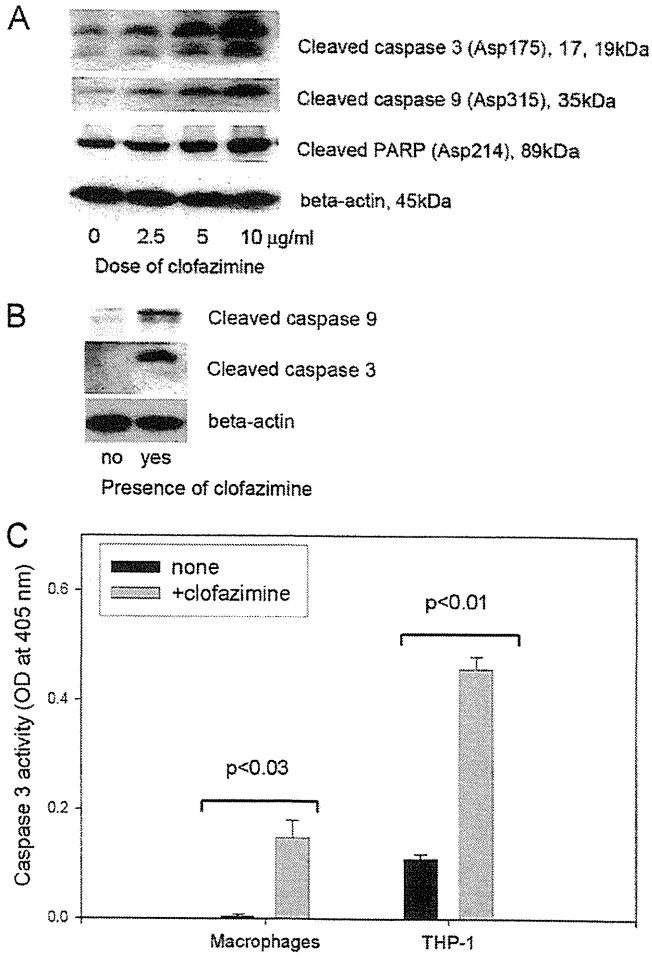

FIG. 5. Expression of caspase in clofazimine-treated THP-1 cells and macrophages. THP-1 cells were incubated in the presence of the indicated concentrations of clofazimine for 6 h, and cell lysates were processed for detection of cleaved caspase-3, caspase-9, and PARP by Western blotting (A). Similarly, monocyte-derived macrophages were incubated in the presence of 10 μg/ml of clofazimine, and the cell lysates were examined for cleaved caspase-3 and caspase-9 expression (B). The caspase activity in clofazimine-treated macrophages and THP-1 cells was analyzed. Macrophages were incubated in the presence of 10 μg/ml of clofazimine for 6 h, and the caspase-3 activity in the cell lysates was determined by colorimetric assay (C). The results are representative of three independent cell culture tests.

demonstrated, suggesting that DNA endonuclease was activated causing apoptosis.

We observed that *M. leprae* by itself does not induce apoptosis of human cells. Similarly, infection of mouse macrophages with viable *M. leprae* was shown not to induce apoptosis (11). Although apoptosis is induced when macrophages infected with *M. leprae* are treated with clofazimine, the host cell viability does not change significantly in the presence of *M. leprae*. Nevertheless, the viability of *M. leprae* in macrophages was significantly lower in clofazimine-treated cells than infected cells not treated with clofazimine (data not shown). Therefore, we can speculate that clofazimine induces apoptosis of *M. leprae*-infected macrophages, which in turn inhibits *M. leprae* growth.

Consequently, we investigated the pathways involved in the execution of macrophage apoptosis (6, 14). We observed enhanced expression of cleaved caspase-3, caspase-9, and PARP following clofazimine treatment in THP-1 cells (Fig. 5A). Colorimetric assay also indicated enhanced caspase-3 activity in both macrophages and THP-1 cells treated with clofazimine (Fig. 5C), suggesting the involvement of caspases in clofazimine-induced apoptosis.

Apoptosis has been shown to be effective in therapy of chronic inflammatory diseases (16). An immunomodulatory drug, thalidomide, is used for treatment of ENL in leprosy patients, and its anti-inflammatory activity is believed to be through the downregulation of production of the proinflammatory cytokine TNF-α (19). Gockel et al. showed that thalidomide induces apoptosis in human monocytes (8). Clofazimine

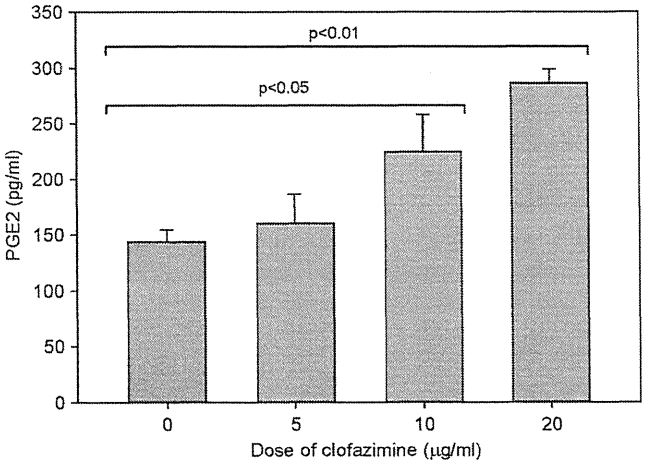

FIG. 6. Enhancement of PGE_2 production by clofazimine in *M. leprae*-infected macrophages. Macrophages were preincubated in the presence of the indicated doses of clofazimine for 4 h, followed by infection with *M. leprae* (5×10^6/well), and the culture was continued for another 20 h. The amount of PGE_2 in the culture supernatants was measured. The results are representative of three independent cell culture tests.

is known to have a favorable influence on the reversal reaction in human leprosy (2). Browne and Hogenzeil found that clofazimine controlled persistent exacerbations in patients who were corticosteroid dependent for controlling the passing reactions, including ENL, and suggested that the drug may exert a suppressive effect on the development of acute exacerbation in lepromatous leprosy (3). These observations have been followed by those of later workers, and one of the special indications for use of clofazimine is the presence of acute reactions or a chronic recurrent reaction in lepromatous leprosy. These clinical data suggest that the mechanisms underlying the action of the drug in these leprosy patients mainly seem to be anti-inflammatory, although there is no direct evidence. Macrophages are capable of elaborating a series of biochemical products with potent immunomodulatory activities. We have observed enhancement of the production of PGE_2, when macrophages were pretreated with clofazimine. PGE_2 is released from arachidonic acid by PLA2. The enzyme is reported to be stimulated in clofazimine-treated neutrophils (10). With respect to B-cell function, prostaglandins of the E series (PGE) inhibit both B-cell proliferation and the generation of antibody-forming cells, and also, B-cell tolerance is induced by PGE_2 (9, 24). T-cell proliferation is also suppressed by PGE_2 (13). The reaction to leprosy involves antibody (ENL caused by immune complex) and cells (delayed-type hypersensitivity mediated mainly by T cells). The mechanisms underlying the immunomodulatory role of clofazimine are still not clear, but the present study clarifies certain aspects. Apoptosis induced in macrophages might explain the anti-inflammatory activities of clofazimine *in vivo*.

In conclusion, our findings suggest that clofazimine induced apoptosis of macrophages through the activation of caspases. The data indicate that the action of clofazimine in leprosy patients may be at least partially mediated by apoptosis.

ACKNOWLEDGMENTS

The study was partly supported by a Research on Emerging and Re-Emerging Infectious Diseases Grant in Aid from the Ministry of Health, Labor and Welfare of Japan.

We are grateful to the Japanese Red Cross Society for kindly providing PBMCs from healthy donors.

REFERENCES

1. **Barry, V. C., et al.** 1957. A new series of phenazines (rimino-compounds) with high antituberculosis activity. Nature **179:**1013–1015.
2. **Browne, S. G.** 1965. 'B 663' possible anti-inflammatory action in lepromatous leprosy. Lepr. Rev. **36:**9–11.
3. **Browne, S. G., and L. M. Hogenzeil.** 1962. "B 663" in the treatment of leprosy. Supplementary report of the pilot trial. Lepr. Rev. **33:**182–184.
4. **Chang, Y. T.** 1966. Further studies on B.663 in murine leprosy. Absence of resistance of M. lepraemurium to B.663 and delay in development of resistance to isoniazid. Int. J. Lepr. Other Mycobact. Dis. **34:**1–6.
5. **Chuaprapaisilp, T., and T. Piamphongsant.** 1978. Treatment of pustular psoriasis with clofazimine. Br. J. Dermatol. **99:**303–305.
6. **Fahy, R. J., A. I. Doseff, and M. D. Wewers.** 1999. Spontaneous human monocyte apoptosis utilizes a caspase-3-dependent pathway that is blocked by endotoxin and is independent of caspase-1. J. Immunol. **163:**1755–1762.
7. **Franzblau, S. G., and J. F. O'Sullivan.** 1988. Structure-activity relationships of selected phenazines against *Mycobacterium leprae* in vitro. Antimicrob. Agents Chemother. **32:**1583–1585.
8. **Gockel, H. R., et al.** 2004. Thalidomide induces apoptosis in human monocytes by using a cytochrome c-dependent pathway. J. Immunol. **172:**5103–5109.
9. **Goldings, E. A.** 1986. Regulation of B cell tolerance by macrophage-derived mediators: antagonistic effects of prostaglandin E2 and interleukin 1. J. Immunol. **136:**817–822.
10. **Krajewska, M. M., and R. Anderson.** 1993. An in vitro comparison of the effects of the prooxidative riminophenazines clofazimine and B669 on neutrophil phospholipase A2 activity and superoxide generation. J. Infect. Dis. **167:**899–904.
11. **Lahiri, R., B. Randhawa, and J. L. Krahenbuhl.** 2010. Infection of mouse macrophages with viable *Mycobacterium leprae* does not induce apoptosis. J. Infect. Dis. **201:**1736–1742.
12. **Maeda, Y., T. Mukai, J. Spencer, and M. Makino.** 2005. Identification of an immunomodulating agent from *Mycobacterium leprae*. Infect. Immun. **73:**2744–2750.
13. **Metzger, Z., J. T. Hoffeld, and J. J. Oppenheim.** 1980. Macrophage-mediated suppression. I. Evidence for participation of both hydrogen peroxide and prostaglandins in suppression of murine lymphocyte proliferation. J. Immunol. **124:**983–988.
14. **Nicholson, D. W., et al.** 1995. Identification and inhibition of the ICE/CED-3 protease necessary for mammalian apoptosis. Nature **376:**37–43.
15. **Niwa, Y., T. Sakane, Y. Miyachi, and M. Ozaki.** 1984. Oxygen metabolism in phagocytes of leprotic patients: enhanced endogenous superoxide dismutase activity and hydroxyl radical generation by clofazimine. J. Clin. Microbiol. **20:**837–842.
16. **Pope, R. M.** 2002. Apoptosis as a therapeutic tool in rheumatoid arthritis. Nat. Rev. Immunol. **2:**527–535.
17. **Reddy, V. M., J. F. O'Sullivan, and P. R. Gangadharam.** 1999. Antimycobacterial activities of riminophenazines. J. Antimicrob. Chemother. **43:**615–623.
18. **Rees, R. J.** 1967. Leprosy. A preliminary review of the experimental evaluation of drugs for the treatment of leprosy. Trans. R. Soc. Trop. Med. Hyg. **61:**581–595.
19. **Sampaio, E. P., E. N. Sarno, R. Galilly, Z. A. Cohn, and G. Kaplan.** 1991. Thalidomide selectively inhibits tumor necrosis factor alpha production by stimulated human monocytes. J. Exp. Med. **173:**699–703.
20. **Sandler, E. D., V. L. Ng, and W. K. Hadley.** 1992. Clofazimine crystals in alveolar macrophages from a patient with the AIDS. Arch. Pathol. Lab. Med. **116:**541–543.
21. **Sarracent, J., and C. M. Finlay.** 1982. The action of clofazimine on the level of lysosomal enzymes of cultured macrophages. Clin. Exp. Immunol. **48:**261–267.
22. **Shepard, C. C., and Y. T. Chang.** 1964. Activity of antituberculosis drugs against *Mycobacterium leprae*. Int. J. Lepr. **32:**260–271.
23. **Sukpanichnant, S., et al.** 2000. Clofazimine-induced crystal-storing histiocytosis producing chronic abdominal pain in a leprosy patient. Am. J. Surg. Pathol. **24:**129–135.
24. **Thompson, P. A., D. F. Jelinek, and P. E. Lipsky.** 1984. Regulation of human B cell proliferation by prostaglandin E2. J. Immunol. **133:**2446–2453.
25. **Wadee, A. A., R. H. Kuschke, and T. G. Dooms.** 1995. The inhibitory effects of *Mycobacterium tuberculosis* on MHC class II expression by monocytes activated with riminophenazines and phagocyte stimulants. Clin. Exp. Immunol. **100:**434–439.
26. **Watson, S. R., L. K. Auclair, and F. M. Collins.** 1981. The effect of combined chemotherapy on suppressor T-cell activity in *Mycobacterium simiae*-infected mice. Immunology **43:**459–465.

JOURNAL OF CLINICAL MICROBIOLOGY, Feb. 2011, p. 613–617
0095-1137/11/$12.00 doi:10.1128/JCM.00817-10

Vol. 49, No. 2

Multiple Cases of Cutaneous *Mycobacterium massiliense* Infection in a "Hot Spa" in Japan[▽]

Kazue Nakanaga,[1]* Yoshihiko Hoshino,[1] Yuko Era,[2] Kentaro Matsumoto,[2] Yuji Kanazawa,[3] Atsuko Tomita,[3] Masanari Furuta,[3] Motohisa Washizu,[4] Masahiko Makino,[1] and Norihisa Ishii[1]

Leprosy Research Center, National Institute of Infectious Diseases, Tokyo 189-0002,[1] Department of Dermatology, Shizuoka Saiseikai General Hospital, Shizuoka 422-0821,[2] Shizuoka City Institute of Environmental Sciences and Public Health, Shizuoka 422-8072,[3] and Shizuoka City Public Health Center, Shizuoka 420-0846,[4] Japan

Received 23 April 2010/Returned for modification 2 August 2010/Accepted 7 December 2010

Seven body polishers working in the same "hot spa" presented with multiple red nodules and papules on their hands and forearms. A causative agent was successfully isolated from two of the subjects and from a swab sample collected from the underside of a bed cover in the body-polishing facility. The two cutaneous isolates and the environmental isolate were rapidly growing mycobacteria that formed nonphotochromogenic smooth or smooth/rough colonies on Ogawa egg slants. They were identified as *Mycobacterium massiliense* by multigenotypic analysis using the 16S rRNA, *hsp65*, and *rpoB* genes and the 16S–23S rRNA internal transcribed spacer (ITS) region. However, the use of the 16S rRNA gene sequence and/or DNA-DNA hybridization (DDH Mycobacteria Kit) alone would not distinguish *M. massiliense* from mycobacteria in the *M. chelonae-M. abscessus* group. The three isolates were significantly more susceptible to clarithromycin, doxycycline, and minocycline than the *M. abscessus* and *M. bolletii* reference strains. One cutaneous isolate and the environmental isolate were in a related cluster by randomly amplified polymorphic DNA PCR (RAPD-PCR). Of the several mycobacterial species found in the day spa, only *M. massiliense* was isolated from biopsy specimens of the skin lesions, suggesting that this bacterium is a human skin pathogen. This is the first known report of cutaneous *M. massiliense* infections that could not be attributed to a prior invasive procedure. This is also the first report of *M. massiliense* infection in Japan.

Mycobacterium massiliense was initially isolated from the sputum of a patient with pneumonia in France in 2004 (1). Epidemiologically, *M. massiliense* has been recognized as an emerging pathogen in the United States (16, 24) and Brazil, where outbreaks have been associated with postsurgical and cosmetic procedures (2, 4, 22). In Korea, an outbreak was linked to intramuscular injections of an antimicrobial agent (9). This bacterium was also the source of a lethal case of sepsis in Italy and has been found in cystic fibrosis patients in France (15, 20). Among pulmonary *M. abscessus* group isolates, almost half of the isolates in Korea and 30% of those in the Netherlands are *M. massiliense* (8, 21). It has been suggested that *M. massiliense* should be reclassified taxonomically as a subspecies of *M. abscessus* (11). The clinical significance of differentiating these two species has also been explored (7). However, *M. massiliense* has not been fully characterized. Although mycobacteria are a frequent source of dermal infection, *M. massiliense* has never been reported as an etiological agent. This report describes the first case of an *M. massiliense* dermal infection in Japan.

Case Reports

In November 2007, a 49-year-old female who worked as a body polisher in a hot spa developed multiple red nodules and papules on her hands and forearms. The number of lesions gradually increased over several months, precipitating a visit to a local hospital in June 2008 (case 1). A skin biopsy specimen of a nodule stained with hematoxylin and eosin (H&E) revealed that the lesion was a structured form of granuloma that contained giant cells and infiltrating lymphocytes with necrosis. Acid-fast bacilli were identified by Ziehl-Neelsen staining.

In October 2008, multiple red nodules and papules appeared on the hands and forearms of a 26-year-old female who worked in the same body-polishing facility as the individual with case 1. She visited the same local hospital in December 2008 (case 2) and received similar biopsy results: acid-fast bacilli and granuloma formation with giant cells and infiltrating lymphocytes.

In addition to cases 1 and 2, in the same spa during the same period, there were five more puzzling cases of body polishers with similar symptoms. Three of these patients (with cases 3 to 5) visited the hospital. However, the presence of acid-fast bacilli was not confirmed, even after the observation of granulomas in the skin biopsy specimen of case 3. In April 2009, environmental sampling was conducted at this hot spa in order to discover the causative agent(s).

MATERIALS AND METHODS

Identification and characterization of isolates. Skin samples were decontaminated with *N*-acetyl-L-cysteine sodium hydroxide (NALC-NaOH) (13). Briefly, an equal volume of NALC-NaOH solution (2% NaOH, 1.45% sodium citrate, 0.5% NALC) was added to as much as 10 ml of a skin specimen homogenized in normal saline. The mixture was vortexed and allowed to stand for 15 to 20 min before neutralization with sterile 0.067 M phosphate buffer (pH 6.8), to a final volume of 50 ml, and centrifugation at 3,000 rpm for 20 min. The supernatant was discarded, and the sediment was resuspended in 2 ml of phosphate-buffered saline. Half of the sediment was stored at −80°C, while the other half was used

* Corresponding author. Mailing address: Department of Mycobacteriology, Leprosy Research Center, National Institute of Infectious Diseases, 4-2-1 Aoba-cho, Higashimurayama-shi, Tokyo 189-0002, Japan. Phone: 81-42-391-8211. Fax: 81-42-394-9092. E-mail: nakanaga@nih.go.jp.

▽ Published ahead of print on 15 December 2010.

TABLE 1. Primers used in this study

Primer	Sequence (positions)	Target and/or purpose (amplified fragment size)	Reference
8F16S	5′-AGAGTTTGATCCTGGCTCAG-3′ (8–27)[a]	16S rRNA gene, PCR (ca. 1,500 bp), sequencing	17
1047R16S	5′-TGCACACAGGCCACAAGGGA-3′ (1047–1028)[a]		
830F16S	5′-GTGTGGGTTTCCTTCCTTGG-3′ (830–849)[a]		
1542R16S	5′-AAGGAGGTGATCCAGCCGCA-3′ (1542–1523)[a]		
TB11	5′-ACCAACGATGGTGTGTCCAT-3′	*hsp65*, PCR (441 bp), sequencing	19
TB12	5′-CTTGTCGAACCGCATACCCT-3′		
MabrpoF	5′-GAGGGTCAGACCACGATGAC-3′ (2112–2131)[b]	*rpoB*, PCR (449 bp), sequencing	This study
MabrpoR	5′-AGCCGATCAGACCGATGTT-3′ (2559–2541)[b]		
ITSF	5′-TTGTACACACCGCCCGTC-3′	16S–23S ITS region, PCR (ca. 340 bp), sequencing	14
ITSR	5′-TCTCGATGCCAAGGCATCCACC-3′		
OPA2	5′-TGCCGAGCTG-3′	RAPD-PCR	25
OPA18	5′-AGGTGACCGT-3′		
INS-2	5′-GCGTAGTGCGTCGGTGACAAA-3′		

[a] Nucleotide positions were assigned using the *Escherichia coli* 16S rRNA gene sequence as a reference.
[b] Primer design and nucleotide positions were based on the *M. tuberculosis rpoB* gene sequence (GenBank/EMBL/DDBJ accession no. L27989).

for acid-fast staining and inoculation into a 2% Ogawa egg slant (case 1) or Middlebrook 7H9 broth enriched with 10% oleic acid-albumin-dextrose-catalase (OADC; Nippon Becton Dickinson, Fukushima, Japan) (7H9 broth) (case 2). Mycobacterial isolates were subcultured on Middlebrook 7H11 agar plates enriched with 10% OADC (Nippon Becton Dickinson) for more than 3 days at 36.5°C.

A total of 15 environmental samples were collected from the body-polishing facility in sterile containers or bags. There were four water samples from different bathtubs, eight swab samples, and three scurf scrub equipment samples (two gloves and one brush). All samples were centrifuged at 3,000 rpm for 20 min to concentrate any organisms; the swab and equipment samples were stirred in sterile normal saline before centrifugation. Following centrifugation, precipitated samples were resuspended in normal saline and were added to 1.5 volume of 1 N hydrogen chloride. After incubation for 20 min, the samples were neutralized with 1 N NaOH. The mixture was centrifuged at 3,000 rpm for 20 min, and the sediment was resuspended in 1 ml of phosphate-buffered saline (5). Suspensions were inoculated onto 2% Ogawa egg slants or into 7H9 broth and were incubated at 36.5°C. Mycobacterial isolates were subcultured on Middlebrook 7H11 agar for more than 3 days at 36.5°C. The characteristics of the cultured isolates were determined as described previously (3).

DNA-DNA hybridization. DNA-DNA hybridization was performed with a DDH Mycobacteria Kit (Kyokuto Pharmaceutical Industrial Co., Tokyo, Japan) to identify mycobacterial species (10). In brief, one-half loopful of a mycobacterial colony was used for the test. Biotin-labeled denatured DNA was extracted from a colony and was distributed into the wells of a microdilution plate where the single stranded DNA from 18 reference strains had been immobilized. After a 2-h hybridization at 55°C, hybridized DNA was detected with peroxidase-conjugated streptavidin and the substrate tetramethylbenzidine. The optical density at 630 nm was measured for each well within 30 min. The labeled strain was identified as one of the 18 species when the maximum color intensity was 1.9 times higher than the intensity of the negative control and the second strongest color intensity was lower than 70% of the maximum color intensity.

DNA extraction. One loopful of a mycobacterial colony on solid medium was suspended in 400 μl sterilized phosphate-buffered saline supplemented with 0.05% Tween 80 and was stored at −80°C until DNA was extracted. A frozen mycobacterial sample was crushed in a bead-beating instrument (Magnalizer; Roche Diagnostics) at 3,000 rpm for 90 s with zirconia beads (diameter, 2 mm). Total genomic DNA was purified from the crushed suspension using the High Pure PCR template preparation kit according to the manufacturer's instructions (Roche Diagnostics) and was stored at −20°C.

Sequence and phylogenetic analysis. Sequences of clinical and environmental isolates, which had been preliminarily identified as *M. abscessus* by the DDH Mycobacteria Kit, were compared to those of the reference strains *M. massiliense* JCM 15300^T, *M. chelonae* JCM 6388^T, *M. abscessus* JCM 13569^T, and *M. bolletii* JCM 15297^T, obtained from the Japan Collection of Microorganisms of the Riken BioResource Center (BRC-JCM; Saitama, Japan). The majority of the 16S rRNA gene, the partial *hsp65* and *rpoB* genes, and the internal transcribed spacer (ITS) region between the 16S and 23S rRNA genes were amplified by PCR using AmpliTaq Gold polymerase (Applied Biosystems, Foster City, CA) with the primers listed in Table 1. Both strands were sequenced with the BigDye Terminator cycle sequencing kit, version 3.1 (Applied Biosystems), and were run on the ABI Prism 310 genetic analyzer (Applied Biosystems) (13). Analyses were performed after removal of the primers from the sequences.

Similarity searches were performed in the DNA Data Bank of Japan (DDBJ) (6). Phylogenetic analyses were performed using the MEGA software package, version 4.0.2 (Build no. 4028) (18). The tree was constructed using the neighbor-joining method with Kimura's two-parameter distance correction model with 1,000 bootstrap replications.

RAPD-PCR. Randomly amplified polymorphic DNA PCR (RAPD-PCR) (25) was performed with three random primers in order to compare clinical and environmental isolates with the *M. massiliense* JCM 15300^T reference strain (Table 1). In brief, 50 μl of a mixture containing 60 mM Tris-HCl (pH 9.0), 2.5 mM $MgCl_2$, 15 mM $(NH_4)_2SO_4$, 250 μM each deoxynucleoside triphosphate (dNTP), 50 pmol of the primer, 1 U of *Taq* DNA polymerase (Takara Bio Inc., Japan), and 100 ng of total genomic DNA, which was freshly extracted or stored for as long as 30 days at −20°C, was used for the PCR. Amplification was performed in the Takara PCR thermal cycler SP using 40 cycles of 94°C for 1 min, 36°C for 1 min, and 72°C for 2 min. The PCR products were separated in the same run by 2% agarose gel electrophoresis and ethidium bromide staining. Strains were assigned to the same cluster when the same band patterns were observed with the three primers or one major band difference was observed in only one of the three primers.

Drug susceptibility assays. Drug susceptibility assays were performed with 7H9 broth microdilutions according to the Clinical and Laboratory Standards Institute (CLSI) guidelines (23), with a modification in drug choice for rapidly growing mycobacteria. Amikacin (AMK), azithromycin (AZM), ciprofloxacin (CIP), clofazimine (CLF), clarithromycin (CLR), doxycycline (DOX), meropenem (MEM), minocycline (MIN), and panipenem (PAPM) were tested against the clinical and environmental isolates and the *M. abscessus*, *M. massiliense*, and *M. bolletii* reference strains. AZM was provided by Pfizer Japan Inc.; MEM and PAPM were provided by Dainippon Sumitomo Pharma Co. Ltd. and Daiichi Sankyo Co. Ltd., respectively; and the other drugs were purchased from Sigma-Aldrich Co. MIC testing was carried out in triplicate on different days, with two of three matching MICs used as the criteria for MIC determination. Susceptibility was evaluated according to the CLSI breakpoint recommendations.

Nucleotide sequence accession numbers. The DNA sequences of the 16S rRNA (1,468 bp), *hsp65* (401 bp), *rpoB* (409 bp), and ITS (298 bp) fragments from the reference strains (*M. massiliense* JCM 15300^T, *M. chelonae* JCM 6388^T, *M. abscessus* JCM 13569^T, and *M. bolletii* JCM 15297^T) and the clinical and environmental isolates have been deposited in the International Nucleotide Sequence Databases (INSD) through the DDBJ under accession numbers AB548592 to AB548611.

TABLE 2. Similarities of nucleotide sequences between case isolates and reference strains of closely related mycobacterial species

Isolate	Species for comparison[a]	% Identity			
		16S rRNA (1,468 bp)	*hsp65* (401 bp)	*rpoB* (409 bp)	ITS (298 bp)
Isolate 1	*M. abscessus*	99.9	98.8	97.6	99.0
	M. massiliense	99.9	100	100	100
	M. bolletii	99.9	99.3	98.3	99.0
	M. chelonae	99.8	92.5	96.1	89.9
Isolate 2	*M. abscessus*	99.9	98.8	97.6	99.0
	M. massiliense	99.9	100	100	100
	M. bolletii	99.9	99.3	98.3	99.0
	M. chelonae	99.8	92.5	96.1	89.9
Environmental isolate	*M. abscessus*	99.9	98.8	97.6	99.0
	M. massiliense	99.9	100	100	100
	M. bolletii	99.9	99.3	98.3	99.0
	M. chelonae	99.8	92.5	96.1	89.9

[a] Reference strains used for comparison were *M. abscessus* JCM 13569^T, *M. massiliense* JCM 15300^T, *M. bolletii* JCM 15297^T, and *M. chelonae* JCM 6388^T.

RESULTS

Isolation from skin and environmental samples. Bacteria isolated from the skin biopsy specimens of cases 1 and 2 were provisionally identified as *M. abscessus* by the DDH Mycobacteria Kit. None of the four environmental samples from the bathtubs yielded mycobacteria. However, mycobacteria grew from four swabs and two gloves used for the scurf scrub. The swab isolate from the underside of the bed cover in the body-polishing room was tentatively identified as *M. abscessus* by the DDH Mycobacteria Kit. The five remaining mycobacterial isolates included *M. nonchromogenicum*, from the stone wall of the body-polishing room; *M. terrae*, from a glove; and three *M. fortuitum* isolates (one from the spring spout, one from the wood wall of the body-polishing room, and one from a glove).

The clinical and environmental (bed cover) isolates were rapidly growing mycobacteria that formed nonphotochromogenic colonies at 25 to 37°C on 2% Ogawa egg slants and 7H11 agar plates but did not grow at 42°C. The isolates were negative for niacin, nitrate reduction, and Tween 80 hydrolysis and were positive for 5% NaCl tolerance, arylsulfatase (3 days), catalase, and urease. However, differences in colony morphology were observed: isolate 1 and the environmental isolate formed smooth colonies, while isolate 2 produced rough colonies.

Genotypic analysis. Nucleotide sequence analysis was performed with the three isolates and four reference strains (*M. abscessus*, *M. massiliense*, *M. bolletii*, and *M. chelonae*). The sequences of the 1,468-bp fragment of the 16S rRNA gene from the three isolates were identical. Only single or triple mismatches with *M. abscessus*, *M. massiliense*, and *M. bolletii*, or with *M. chelonae*, respectively, were found at nucleotide positions 1008 or 999, 1039, and 1265. The sequences of *hsp65*, *rpoB*, and the ITS region were also identical among the three isolates, showed complete identity with those of *M. massiliense*, and were 89.9 to 99.3% similar to those of *M. abscessus*, *M. bolletii*, and *M. chelonae* (Table 2). Phylogenetic trees, developed using sequences from the *hsp65* and *rpoB* genes, clustered the isolates with *M. massiliense* (Fig. 1), although the clustering was not as clear with trees developed using sequences from the 16S rRNA gene and the 16S-23S rRNA ITS region (data not shown). Confirmation of these three isolates as *M. massiliense* led to the supposition that *M. massiliense* might be the underlying cause of the cutaneous lesions and that the environment of the day spa led to the acquisition of the infections.

Randomly amplified polymorphic DNA PCR. Strain typing was performed by RAPD-PCR with three random primers to clarify the relatedness of the clinical and environmental *M. massiliense* isolates. A comparison of the OPA2 band patterns (Fig. 2, lanes 1 to 4) revealed distinct differences in the amplification patterns of the clinical isolates versus the *M. massiliense* reference strain. The patterns of isolate 1 and the environmental isolate differed by a minor band. The OPA18 and INS-2 band patterns of isolate 1 and the environmental isolate were identical or differed by only one minor band, though these band patterns were clearly different between the clinical isolates and the reference strain (Fig. 2, lanes 5 to 8 and 9 to

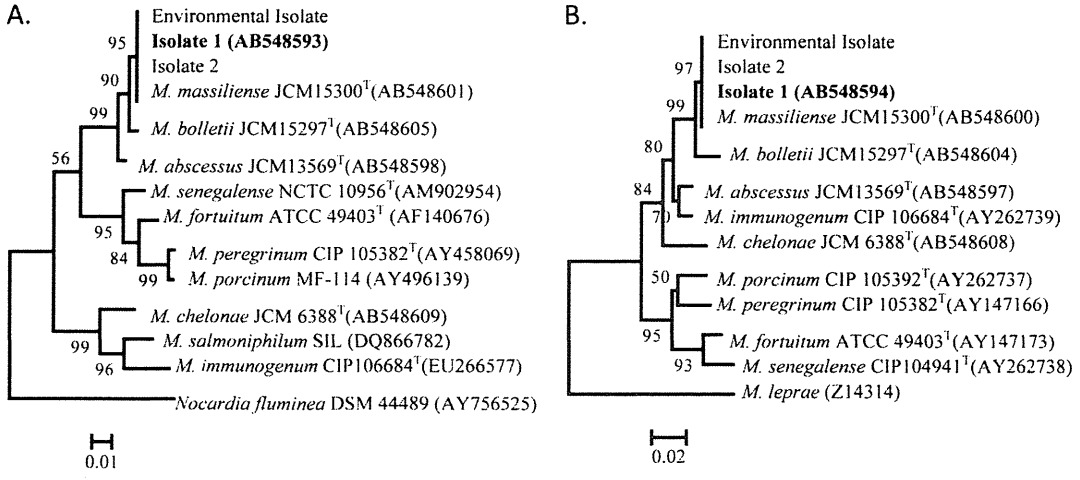

FIG. 1. Phylogenetic analysis based on the *hsp65* (A) and *rpoB* (B) genes of isolate 1 (boldface) and other rapidly growing mycobacteria. The numbers at the nodes are the percentages of bootstrap levels supported by 1,000 resampled data sets. Bootstrap values of <50% are not shown. *Nocardia fluminea* (A) and *M. leprae* (B) were used as outgroups.

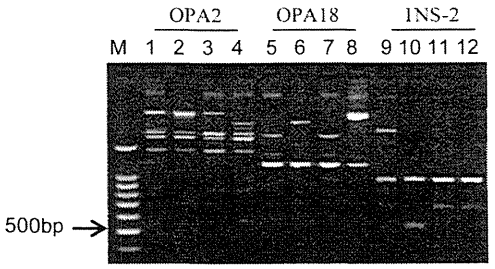

FIG. 2. Comparison of the RAPD-PCR patterns of the clinical isolates (isolates 1 and 2), the environmental isolate, and a reference strain (*M. massiliense* JCM 15300^T) with three different primers. Lanes 1, 5, and 9, DNA from isolate 1; lanes 2, 6, and 10, DNA from isolate 2; lanes 3, 7, and 11, DNA from the environmental isolate; lanes 4, 8, and 12, DNA from the *M. massiliense* reference strain; lane M, DNA size marker (100-bp ladder). RAPD-PCR patterns produced with primers OPA2 (lanes 1 to 4), OPA18 (lanes 5 to 8), and INS-2 (lanes 9 to 12) are shown.

12). Therefore, isolate 1 and the environmental isolate were assigned to the same cluster by RAPD-PCR analysis but were different from isolate 2.

Assays for susceptibility to antimicrobial agents. The results of tests of the susceptibilities of the clinical and environmental isolates to antimicrobial agents are shown in Table 3. All three isolates exhibited susceptibility patterns similar to that of the *M. massiliense* reference strain (1, 11, 16), such as susceptibility to clarithromycin, minocycline, doxycycline, and amikacin and resistance to ciprofloxacin. The strains were also tested against azithromycin, clofazimine, meropenem, and panipenem, though these were not on the list of CLSI-recommended drugs (23). Notably, the MICs of azithromycin for the three isolates and the *M. massiliense* reference strain were lower than those for the *M. abscessus* and *M. bolletii* reference strains. No differences in the MIC were observed with clofazimine, meropenem, and panipenem.

DISCUSSION

In 2004, *M. massiliense* was proposed as a new species in the *M. chelonae-M. abscessus* group (1). Its 16S rRNA gene had complete identity with that of *M. abscessus* and more than 99.6% similarity with the *M. chelonae* and *M. immunogenum* genes. Therefore, genotypic analysis using single-target sequencing of the 16S rRNA gene would not distinguish *M. massiliense* from other mycobacteria in the *M. chelonae-M. abscessus* group. Two independent groups have reported on the inaccuracy of single-target sequencing for the diagnosis of *M. massiliense* (11, 12). Similarly, the DDH Mycobacteria Kit could not distinguish *M. massiliense* from *M. abscessus*, because the objective species of this kit were limited to 18 mycobacterial species: *M. tuberculosis*, *M. kansasii*, *M. marinum*, *M. simiae*, *M. scrofulaceum*, *M. gordonae*, *M. szulgai*, *M. avium*, *M. intracellulare*, *M. gastri*, *M. xenopi*, *M. nonchromogenicum*, *M. terrae*, *M. triviale*, *M. fortuitum*, *M. chelonae*, *M. abscessus*, and *M. peregrinum*. However, with this kit, the one isolate provisionally identified as *M. abscessus* was easily distinguished from several environmental surveillance mycobacterial isolates.

The appearance of skin lesions among day spa workers led to the collection and analysis of workplace environmental samples. Although environmental surveillance was performed several months after case 1 first presented with symptoms, RAPD-PCR showed that isolate 1 and the environmental isolate were part of the same cluster (Fig. 2). In contrast, the same analysis revealed that isolate 2 belonged to a different cluster. The relationship between isolate 1 and the environmental isolate suggests that the unhygienic conditions in the day spa led to the acquisition of the infections, but the cause and effect could not be resolved, because the origin of isolate 2 was not specified. RAPD-PCR typing also showed that the *M. massiliense* reference strain isolated in France had a different amplification pattern, which was indicative of the geographical distinction between the Japanese and French isolates.

Based on published reports, this is the first presentation of cutaneous *M. massiliense* infections that were not preceded by an invasive procedure. *M. massiliense* may be more pathogenic to human skin than other species, since only *M. massiliense* was isolated from the skin biopsy specimens, though several species of mycobacteria were isolated from the day spa facility. The antimicrobial susceptibility profile of *M. massiliense* is shown in Table 3. Further studies are required to determine if the profile differs from those of other members of the *M. chelonae-M. abscessus* group and if any differences can be used as a typing tool. Interestingly, the MICs of azithromycin, clarithromycin,

TABLE 3. Results of drug susceptibility tests

Antimycobacterial drug[a]	MIC (μg/ml) for:					
	Isolate 1	Isolate 2	Environmental isolate	*M. massiliense* JCM 15300^T	*M. abscessus* JCM 13569^T	*M. bolletii* JCM 15297^T
AMK	16	16	16	16	16	16
AZM	16	32	16	16	64	128
CIP	8	16	8	8	8	8
CLF	1	2	1	2	1	2
CLR	0.25	0.25	0.25	0.25	4	4
DOX	2	8	1	1	64	64
MEM	8	8	16	8	16	8
MIN	1	2	0.5	0.5	16	8
PAPM	64	32	64	64	64	64

[a] AMK, amikacin; AZM, azithromycin; CIP, ciprofloxacin; CLF, clofazimine; CLR, clarithromycin; DOX, doxycycline; MEM, meropenem; MIN, minocycline; PAPM, panipenem.